https://doi.org/10.5194/bg-2019-339
Preprint. Discussion started: 3 September 2019

Biogeosciences Discussions
Open Access
EGU

Is deoxygenation detectable before warming in the thermocline?

Angélique Hameau[1, 2], Thomas L. Frölicher[1, 2], Juliette Mignot[3], and Fortunat Joos[1, 2]

[1]Climate and Environmental Physics, Physics Institute, University of Bern, Switzerland
[2]Oeschger Centre for Climate Change Research, Bern, Switzerland
[3]LOCEAN/IPSL, Sorbonne Université (SU)-CNRS-IRD-MNHN, Paris, France

Correspondence: Angélique Hameau (hameau@climate.unibe.ch)

Abstract. Multiple lines of evidence from observation- and model-based studies show that anthropogenic greenhouse gas emissions cause ocean warming and oxygen depletion, with adverse impacts on marine organisms and ecosystems. Temperature is considered as one of the main indicators of climate change, but, in the thermocline, anthropogenic changes in biogeochemical tracers such as oxygen may emerge from the bounds of natural variability before changes in temperature. Here, we compare the local time of emergence (ToE) of anthropogenic temperature and oxygen changes in the thermocline within an ensemble of Earth system model simulations from the fifth phase of the Coupled Model Intercomparison Project (CMIP5). Anthropogenic deoxygenation emerges from natural internal variability before warming in 35±11% of the global thermocline. Earlier emergence of oxygen than temperature change is simulated by all models in parts of the subtropical gyres of the Pacific and the Southern Ocean. Earlier detectable changes in oxygen than temperature are typically related to decreasing trends in ventilation. The supply of oxygen-rich surface waters to the thermocline is reduced as evidenced by an increase in apparent oxygen utilisation over the simulations. Concomitantly, the propagation of the warming signal is hindered by slowing ventilation, which delays the warming in the thermocline. As the magnitudes of internal variability and simulated temperature and oxygen changes, which determine ToE, vary considerably among models, we compute the local ToE relative to the global mean ToE within each model. This reduces the inter-model spread in the relative ToE compared to the traditionally evaluated absolute ToE. Our results underline the importance of an ocean biogeochemical observing system and that the detection of anthropogenic impacts becomes more likely when using multi-tracer observations.

https://doi.org/10.5194/bg-2019-339
Preprint. Discussion started: 3 September 2019

Biogeosciences Discussions Open Access EGU

1 Introduction

Carbon emissions from human activities are causing ocean warming (Rhein et al., 2013) and ocean deoxygenation, i.e. a decrease in the oceanic oxygen (O_2) concentration (Sarmiento et al., 1998; Bopp et al., 2002; Matear and Hirst, 2003; Battaglia and Joos, 2018). Both warming and deoxygenation adversely affect marine organisms and ecosystems and the services they provide (e.g. Pörtner et al., 2014; Deutsch et al., 2015; Gattuso et al., 2015; Magnan et al., 2016).

All major ocean basins have experienced a significant warming over the last few decades. Warming is generally strongest at the surface and weaker at deeper layers, indicative of heat penetrating from the surface towards the deep ocean as expected from atmospheric greenhouse gas forcing. The strongest warming in the top 2000 m has been observed in the Southern Ocean (Roemmich et al., 2015) and the tropical/subtropical Pacific and Atlantic Ocean (Cheng et al., 2017). On regional to local scale, the anthropogenic warming signal may be masked by natural interannual to multi-decadal variability. For example, decadal-scale cooling trends in the tropical Pacific and Indian oceans may arise from natural El Nino-Southern Oscillation and/or Indian Ocean Dipole variability (Han et al., 2014). Similarly, decadal variability in the Atlantic Meridional Overturning is observed to modulate temperature and heat content change in the North Atlantic (Chen and Tung, 2018). Global climate models, such as the Earth system models that participated in phase 5 of the Coupled Model Intercomparison Project (CMIP5) reproduce the long-term trend in global ocean heat content over the last 50 years when uncertainties of observation-based estimate and internally generated natural variability are taken into account (Frölicher and Paynter, 2015; Cheng et al., 2019).

Concomitant with ocean warming, observation-based studies indicate that the global ocean oxygen content has decreased since 1960 (e.g. Schmidtko et al., 2017). Increased ocean surface temperature reduces oxygen solubility, limiting atmospheric oxygen dissolution into the upper ocean. In subsurface waters, oxygen concentration is also affected by ventilation, remineralisation of organic matter and air-sea disequilibrium but the oxygen decrease is mostly dominated by a reduction in ventilation and increased consumption (Bopp et al., 2002, 2017; Hameau et al., 2019). The largest losses are located in the Pacific Ocean (equator and northern hemisphere) and the Southern Ocean. However, observations are relatively sparse and only start during the late industrial period. It remains therefore still difficult to precisely distinguish human caused trends from natural variations in O_2. Modelling studies also agree on the sign of oceanic O_2 changes, but likely underestimate the magnitude of loss (Cocco et al., 2013; Bopp et al., 2013). In particular in the tropical regions, models are not able to reproduce observed O_2 decrease in equatorial low-oxygen zones (Stramma et al., 2008; Cocco et al., 2013; Cabré et al., 2015).

It is expected that ocean warming and deoxygenation, and the combination thereof, increases the risk of adverse impacts on marine organisms and ecosystem services (Pörtner et al., 2014). Warming of the ocean influences the physiology and ecology of almost all marine organisms. Reduced oceanic O_2 concentrations can disrupt marine ecosystems by pushing organisms to their species-specific limits of hypoxic tolerance, below which the species are no longer able to meet their metabolic O_2 demand. The species-specific metabolic demand of O_2 is also a function of temperature, as warmer temperatures increase metabolic rates and oxygen requirements. At the same time, higher ocean temperatures also decrease oxygen supply through reduced ventilation, enlarging the regions with limited O_2 concentrations and thus shifting ecosystem distribution (Cheung et al., 2011).

https://doi.org/10.5194/bg-2019-339
Preprint. Discussion started: 3 September 2019

Beyond the combined impact of physical and biogeochemical changes, an interesting question is whether anthropogenic changes in the ocean are first detectable in physical variables such as temperature (T) or in biogeochemical variables such as O_2, pH, or DIC (Joos et al., 2003; Keller et al., 2015). The answer may have implications for measurement strategies to detect anthropogenic changes as well as for the impacts of physical and biogeochemical change on marine life. On the one hand, physical processes generally influence the biogeochemistry of the ocean. For example, global warming increases surface ocean temperature, which reduces O_2 solubility and decreases air-sea gas exchange of O_2. On the other hand, O_2 is also influenced by non-thermal processes, such as respiration and the redistribution by ocean circulation and mixing. Respiration of organic matter in the ocean interior will have a larger influence on O_2 in a more stratified and less ventilated ocean. One could therefore expect that, under global warming, the combined effect of increased O_2 consumption and decreased O_2 solubility will accelerate the O_2 depletion in subsurface waters and that O_2 be detectable before the warming reaches that layer.

In the context of climate change, the distinction between anthropogenic induced changes and natural variability is pivotal to gain understanding on O_2 and temperature changes. The concept of Time of Emergence (ToE; Christensen et al., 2007; Hawkins and Sutton, 2012) is often used to determine the point in time when the anthropogenic signal becomes larger than natural variability. ToE has been broadly used in climate change detection for physical climate variables (e.g. surface temperature: Hawkins and Sutton, 2012; Frame et al., 2017), land carbon fluxes (Lombardozzi et al., 2014) or marine biogeochemical variables (e.g. pH, alkalinity, DIC, pCO_2: Hauri et al., 2013; Keller et al., 2014; marine biological productivity: Henson et al., 2016). A limited number of studies addressed anthropogenic deoxygenation detection in the subsurface layers (Rodgers et al., 2015; Frölicher et al., 2016; Henson et al., 2016; Long et al., 2016; Henson et al., 2017; Hameau et al., 2019). Only one study (Hameau et al., 2019), using a single model, investigated ToE of temperature in the thermocline. One main finding of their study is that anthropogenic driven ocean warming emerges much earlier than the O_2 signal in low and midlatitude regions. This is due to the opposite effect of decreases in O_2 solubility and O_2 consumption, delaying the O_2 changes. In the high latitudes and the Pacific subtropical gyres, deoxygenation emerges before ocean warming in their model. This is because the decrease in oxygen solubility is reinforced by an increase in O_2 consumption, leading to strong O_2 depletion.

Even though this earlier study indeed identifies regions with earlier emergence of O_2 in comparison with temperature, consistent with our outlined hypothesis above, it is currently unclear if this single-model result is robust across a suite of different Earth system model simulations. A multi-model study that addresses and compares the emergence of anthropogenic warming and of deoxygenation in the thermocline is currently missing. However, such a comparison across models is delicate, as the absolute years of emergence (Keller et al., 2014; Henson et al., 2017) is highly dependent of the ToE methodology. We therefore introduce a relative ToE, considered as a deviation relative to the model mean ToE for improved model intercomparison.

In this study, we analyse and compare the relative ToE(T) and ToE(O_2) in the thermocline (200 – 600 m) using nine different CMIP5 Earth system models. We also assess the impact of using the relative ToE in comparison to the classical approach using absolute ToE. In addition, we discuss the magnitude of background internal variability and anthropogenic signal, and their translation into ToE. Finally, we analyse the role of solubility, ventilation and respiration for the emergence of anthropogenic changes in oxygen and temperature.

https://doi.org/10.5194/bg-2019-339
Preprint. Discussion started: 3 September 2019

2 Method

2.1 Earth system models

We use output from eight different configurations of four Earth system models (ESMs) that participated in the Coupled Model Intercomparison Project 5 (CMIP5; Taylor et al., 2012): GFDL-ESM2M, GFDL-ESM2G, HadGEM2-CC, IPSL-CM5A-LR, IPSL-CM5A-MR, IPSL-CM5B-LR, MPI-ESM-LR and MPI-ESM-MR (Table 1). In addition, output from simulations with the Community Earth System Model (CESM1.0) conducted at the Swiss Supercomputing Centre are included in the analysis. The horizontal ocean model resolution is generally about 1° (both GFDL models and CESM1.0). Exceptions are the HadGEM2-CC and IPSL models, which have a horizontal resolution of about 2° and the MPI models, which have a horizontal resolution of about 0.4° (MR) and 1.5° (LR). Of the nine models, all but one (GFDL-ESM2G, isopycnal vertical coordinate) use a pressure-based vertical coordinate. For additional information on the individual model setups, the reader is referred to the references listed in Table 1.

Both the CMIP5 ESMs and the CESM1.0 were run under prescribed anthropogenic and natural greenhouse gas and aerosol forcing. All simulations span the historical 1861-2005 period and the 2006-2100 period following the Representative Concentration Pathway 8.5 (RCP8.5) scenario. The RCP8.5 represents a high emission scenario with a radiative forcing of 8.5 Wm^{-2} in year 2100 (Riahi et al., 2011). These simulations are complemented with output from corresponding control runs with constant preindustrial forcing. The CESM1.0 simulations differ from the CMIP5 simulations only with regard to the spin-up procedure: The CMIP5 model simulations are branched off from preindustrial control simulations, whereas the CESM1.0 simulation is an extension of a last millennium simulation (Lehner et al., 2015). For this study, all CMIP5 models are used for which the 3-d output of oxygen, temperature and salinity for all simulations were available on the Earth System Grid. We regridded all model output onto a 1° x 1° grid. Even though the model drift in the control simulations is relatively small in the thermocline (3.6±2.4 x 10^{-3} $\mathrm{mmol\ m}^{-3}$ year^{-1} for trend in global mean oxygen concentration and 7.2±6.6 x 10^{-5} °C year^{-1} for trend in global mean temperature averaged over 200 – 600 meters), we detrended all model output with a linear trend obtained from the preindustrial control simulation in each grid cell. The CESM1.0 simulation also shows some model drift.Therefore, an exponential curve was fitted to the annual output of its associated control simulation at each grid cell. The detrending procedure is described in detail in Hameau et al. (2019).

2.2 Multi-model analysis methods

We use the concept of Time of Emergence (ToE; e.g. Hawkins and Sutton 2012) to compare anthropogenic changes in O_2 and temperature (signal; S) with internal natural variations (background noise; N). We define the absolute ToE as the first year when the anthropogenic signal S becomes equal or larger than twice the noise of internal natural variability N (Eq. 1; following Hameau et al., 2019).

$$\mathrm{ToE} : \frac{S}{N} \geqslant 2 \tag{1}$$

https://doi.org/10.5194/bg-2019-339
Preprint. Discussion started: 3 September 2019


Biogeosciences Discussions Open Access EGU

We estimate N at each grid cell by calculating one standard deviation (SD) of the annual means in O_2 and T from the preindustrial control simulation. Thus, N represents the noise due to the internal chaotic variability of the climate system. Note that this definition of the noise differs from Hameau et al. (2019), who used internal plus externally-forced natural variability from a last millennium simulation to assess the standard background noise. S is estimated at each grid cell from the forced simulation by fitting the annual evolution of the considered variable with a low-pass filter (cut-off period of 80 years; Enting, 1987) in order to remove short term variations, e.g. associated with internal natural variability. To ensure that S indeed detects anthropogenic trend, we also apply a criterion for the sign of S to define ToE: S needs to have the same sign as the difference between the last 30 years of the future simulation and the preindustrial average for the corresponding variable and grid cell. Annual O_2 and T data are first averaged over the thermocline (200 – 600 m) at each horizontal grid cell and local S and N are computed from these depth-averaged values for each model, variable and grid-point.

In order to minimise inter-model differences and to highlight the common spatial patterns of ToE, we introduce a new metric, the relative ToE (ToE_{rel}). It is defined as the absolute ToE (ToE_{abs}) minus the global area-averaged ToE (ToE_{glob}; Eq. 2).

$$ToE_{rel} = ToE_{abs} - ToE_{glob} \quad (2)$$

Median and spread (interquartile range) of the multi-model estimations are computed from the annual outputs of the model ensemble and uniform weights are applied to each model configuration to compute those statistics. Tests have been performed using a weighted median as several simulations stem from the same model family (CESM x 1; GFDL x 0.5; HadGEM2 x 1; IPSL x 0.3; MPI x 0.5). However, median and interquartile range of the multi-model ensemble are not sensitive to the weighting scheme applied (not shown). Because an anthropogenic signal may not emerge before the end of the simulation in year 2100, ToE can be undefined. We therefore request that ToE values is defined for at least seven out of nine models to compute the multi-model statistics (median and spread). If more than two models have an undefined ToE, we mask the grid points in maps of the multi-model median and of the multi-model the spread.

To understand the processes behind the simulated changes in ocean O_2, we decompose the O_2 changes into solubility ($O_{2,\,sol}$) or thermal components and Apparent Oxygen Utilisation (AOU) or non-thermal components:

$$[O_2] = [O_{2,\,sol}] + [\text{-AOU}] \quad (3)$$

The solubility component for each model is computed following Garcia and Gordon (1992), which requires local salinity and temperature output. The solubility depends mostly on temperature with a small contribution of salinity. The non-thermal component ([-AOU]) is deduced from the difference between $O_{2,\,sol}$ and O_2 following Eq. 3. In Sect. 3.4, we will use changes in [-AOU] as a proxy for changes in water mass age and ventilation. Output of an ideal age tracer is not available for most models. A decrease in water exchange between the surface ocean and the thermocline typically leads to an increase in water mass age in the thermocline. Therefore, changes in ventilation affect the balance between the rate of supply of O_2-rich waters from the surface and the rate of O_2 consumption by remineralisation of organic matter. It has been demonstrated in earlier studies

https://doi.org/10.5194/bg-2019-339
Preprint. Discussion started: 3 September 2019


Biogeosciences Discussions Open Access EGU

(e.g. Gnanadesikan et al., 2012; Bopp et al., 2017; Hameau et al., 2019) that a decrease in [-AOU] typically corresponds to a decrease in ventilation and an increase in water mass age, as simulated changes in the remineralisation rates of organic material and in associated O_2 consumption are relatively small over the 21st century.

https://doi.org/10.5194/bg-2019-339
Preprint. Discussion started: 3 September 2019


Biogeosciences Discussions Open Access EGU

3 Results

3.1 Relative Time of Emergence

We start by discussing the multi-model median and spread of relative ToE estimates for potential temperature (Fig. 1a, b) and dissolved oxygen (Fig. 1d, e) changes in the thermocline (200 – 600m).

3.1.1 Anthropogenic warming

$ToE_{rel}(T)$ shows early emergence in low latitudes and between 30° S and 60° S, and late emergence in the western tropical Pacific, in the Atlantic subpolar gyre and the subtropical gyres of the Indian and Pacific Ocean (Fig. 1a). The northern Indian Ocean and the eastern equatorial Atlantic stand out as the regions with earliest emergence in anthropogenic warming, i.e. 70 years (median of nine $ToE_{rel}(T)$) before the global average ToE. No emergence by the end of the 21st century (for at least 3 models; cf. Sect. 2.2) is simulated in the subtropical gyres of the Indian and the Pacific oceans, south of Greenland and locally south of 60° S.

The multi-model spread in $ToE_{rel}(T)$ is generally small in regions with early emergence (Fig. 1b). This is the case in many regions of the Pacific and the Southern Ocean (±15 years). However, in the Atlantic subtropical gyres and in the Arabian Sea, the early $ToE_{rel}(T)$ estimates are associated with a wider spread across models (±25 to ±45 years). Large inter-model spread is also found in the Kuroshio extension and in the Indian and Atlantic region of the Southern Ocean (±50 years). In the global average, the multi-model spread for $ToE_{rel}(T)$ is 25 years.

The patterns of $ToE_{rel}(T)$ for each individual model are shown in Fig. 2. As described previously, low latitude regions and parts of the Southern Ocean show earlier emergence compared to mid- and other high-latitude regions. The HadGEM2-CC model (Fig. 2c) is an exception in that respect as temperature emerges later (+30 to +50 years) than the global average in the tropical Atlantic and Pacific. In the Pacific and Indian subtropical gyre regions, the models show late (IPSL family) or no emergence. And finally, CESM and the IPSL family models are the only models that show emergence before the end of the 21st century in the subtropical gyres of the Pacific.

3.1.2 Anthropogenic deoxygenation

In contrast to $ToE_{rel}(T)$, the pattern of $ToE_{rel}(O_2)$ is relatively homogeneous (Fig. 1d) and only varies by about ±40 years between regions. Early emergence is found in the subtropical gyre of the North Pacific, the northern North Atlantic, the Atlantic sector of the Southern Ocean, and generally south of 60° S. No emergence is simulated in 47 % of the ocean area by the end of the 21st century including large parts of the tropics and the subtropical gyres of the Atlantic Ocean and the Indian Ocean.

https://doi.org/10.5194/bg-2019-339
Preprint. Discussion started: 3 September 2019

The multi-model spread for $ToE_{rel}(O_2)$ is 20 years in the global average and thus somewhat smaller than for $ToE_{rel}(T)$. The models show a high spread for $ToE_{rel}(O_2)$ ($\pm$50 years) at low latitudes, such as in the southern Arabian Sea or in the equatorial Atlantic, whereas high model agreement is found in parts of the central North Pacific and the northern Indian Ocean (spread of $\pm$15 years) (Fig. 1e). In the eastern tropical Atlantic, the spread for $ToE_{rel}(O_2)$ is, despite a smaller global mean spread, larger than for $ToE_{rel}(T)$. In summary, even though the median pattern of $ToE_{rel}(O_2)$ is relatively uniform in comparison to $ToE_{rel}(T)$, the spread for $ToE_{rel}(O_2)$ varies between regions as for $ToE_{rel}(T)$.

The multi-model median O_2 signal does not emerge in 47 % of the global thermocline as noted above. Mid and low latitudes show no emergence by the end of the 21st century in most of the models (Fig. 3). However, the exact regions of no emergence differ between models. This regional mismatch, in combination with the requirement that at least seven out of nine models need to show an emerging signal (Sect. 2.2), explains why in the multi-model analysis many grid cells are masked, indicating no emergence in the median (Fig. 1d-f). The area fraction with no emerging O_2 signal is smaller in individual models than in the multi-model median and ranges between 10 and 30 %.

The analysis of $ToE_{rel}(O_2)$ for individual models reveals some additional notable differences (Fig. 3). GFDL-ESM2M, GFDL-ESM2G, HadGEM2-CC and CESM1.0 simulate early emergence in the Southern Ocean, but the IPSL models project no emergence of deoxygenation in this region by the end of the 21st century. In addition, the IPSL models and the CESM1.0 model show relatively early emergence in many grid cells of the western tropical Pacific, a region with no emergence in other models. $ToE_{rel}(O_2)$ also diverges across the models in the Atlantic subtropical gyres: in the HadGEM2 and IPSL simulations, oxygen changes are simulated to emerge relatively early ($ToE_{rel}(O_2) \sim$ 40 to 60 years), whereas in the GFDL, MPI and CESM simulations, the changes are not yet detectable by the end of the 21st century.

3.2 Relative versus absolute ToE

Mapping ToE_{rel} for different models is intended to emphasise common patterns across models by removing the global mean bias between models, while model-model differences in ToE_{abs} are indicative of an overall model uncertainty.
The multi-model spread for ToE_{abs} is by design larger than the multi-model spread for ToE_{rel} for temperature (Fig. 1b, c) and oxygen (Fig. 1e, f), while spatial patterns are similar for ToE_{rel} and ToE_{abs}. On global average, the spread is reduced from $\pm$30 years for $ToE_{abs}(T)$ to $\pm$ 23 years for $ToE_{rel}(T)$ and from $\pm$20 years for $ToE_{abs}(O_2)$ to $\pm$17 years for $ToE_{rel}(O_2)$. Regionally, the reduction can be larger. For example, in the equatorial regions, the Atlantic and the Southern Ocean, the spread is reduced by 20 to 50 years when computed for $ToE_{rel}(T)$ instead for $ToE_{abs}(T)$. Similarly, the spread in $ToE(O_2)$ is reduced from $\pm$35 to $\pm$5 years in parts the North Pacific.

https://doi.org/10.5194/bg-2019-339
Preprint. Discussion started: 3 September 2019

3.3 Internal natural variability and anthropogenic signals

The ToE allows for a comparison across climate models, by combining climate sensitivity to anthropogenic forcing and natural variability in one metric. The magnitude and the spatial patterns of the internal natural variability (SD) and of the anthropogenic signal for both thermocline temperature and oxygen are discussed next.

The multi-model median of internal natural variability for thermocline temperature fluctuates with an amplitude typically ranging between ±0.1 °C in the tropics and the Arctic Ocean, and ±0.5 °C in mid-to-high latitudes (Fig. 4a). SD(T) is the largest (up to ±0.9 °C) in the Western Boundary Currents such as the Kuroshio Current and the Gulf Stream. The variability is also relatively large along the equatorward flanks of the subtropical gyres. It is also in these regions where SD(T) differs most among models (up to ±0.5 °C along the North Atlantic Current; Fig. 4c).

In the multi-model median, temperature in the thermocline is projected to increase on global average by 1.2±0.7 °C (Fig. 4b) by the end of the 21st century under the RCP8.5 scenario relative to the period 1861-1959, in accordance with (Levitus et al., 2009, 2012; Bilbao et al., 2019). Large warming of more than 4.0±0.7 °C is projected in the northern North Atlantic and around the subantarctic water in the Indian and Atlantic Oceans (Fig. 4b and Fig. S4). We note that these regions are also characterised with the largest inter-model spread (±1.5 °C; Fig. 4d and Fig. S4). Finally, disagreement among models in simulating changes in thermocline temperature is also large in the Arctic Ocean, possibly related to different simulated changes in sea ice cover (Stroeve et al., 2012; Wang and Overland, 2012).

The combination of a strong signal and small variability typically results in early detection of the changes. This is the case in the Southern Ocean at 45° S (in the Atlantic and Indian regions; Fig. 1a), where the anthropogenic warming is strong (up to 4 °C; Fig. 4b) but the variability is relatively small (0.1 °C to 0.3 °C; Fig. 4a). However, early emergence of anthropogenic changes can also occur when the signal is relatively small, if the variability is even smaller. This is the case in the tropical oceans such as in the Arabian Sea and the equatorial Atlantic, where water masses warm modestly (up to 1.5 °C), but vary naturally between 0.1 °C and 0.2 °C only.

Natural variability of dissolved oxygen concentrations is particularly large in the northern North Pacific and North Atlantic, the Southern Ocean and along the equatorward boundaries of the subtropical gyres with SD(O_2) of up to 10 $\mathrm{mmol\ m^{-3}}$ (Fig. 5a). The multi-model spread of SD(O_2) (Fig. 5c) is about equally large as the median of SD(O_2) (Fig. 5a) along the equatorward boundaries of the subtropical gyres. Looking at the individual model responses, the O_2 natural variability shows a wide range of different patterns (Fig. S5). The GFDL and MPI models simulate high natural variability of oxygen in the entire thermocline, whereas CESM, HadGEM2 and IPSL models show high variability regionally.

https://doi.org/10.5194/bg-2019-339
Preprint. Discussion started: 3 September 2019


Biogeosciences Discussions Open Access EGU

The O_2 concentration in the thermocline (Fig. 5b) is projected to decrease under global warming, in accordance with previous model studies (e.g. Sarmiento et al., 1998; Cocco et al., 2013; Bopp et al., 2017). The anthropogenic decrease in O_2 is large in the Southern Ocean, in the North Pacific subtropical gyre and in the North Atlantic subpolar gyre. In tropical regions, the changes are projected to be small, except for the western Indian ocean, where more than 70% of the models project an increase of O_2 concentration. The simulated O_2 changes differ most across models in high latitudes and in the subopolar gyres, as well as in the equatorial Indian ocean (Fig. 5d).

Despite differences in the simulated magnitude of O_2 changes and natural variability patterns of O_2 between the different models, the resulting $\mathrm{ToE}_{\mathrm{rel}}(O_2)$ are surprisingly robust across models. For example, the decrease in O_2 spans from -12 to -40 $\mathrm{mmol\,m^{-3}}$ (Fig. S6) and $\mathrm{SD}(O_2)$ spans from ± 5 to ± 15 $\mathrm{mmol\,m^{-3}}$ (Fig. S5) in the central North Pacific. Moreover, the spatial locations of the maximum O_2 depletion differ across the models. However, $\mathrm{ToE}_{\mathrm{rel}}(O_2)$ in this region is within ± 10 years (Fig. 1d), with a relatively high confidence interval (± 10 years). Another example is the CESM model. The very early detection of anthropogenic changes (for temperature and oxygen) in the CESM model described in Sect. 3.1, results from a particularly weak of internal variability (Figs. S3i and S5i; see also Hameau et al., 2019) combined with a high climate sensitivity of the model (Figs. S4i and S6i). Using the $\mathrm{ToE}_{\mathrm{rel}}$ allows the comparison of ToE resulting from CESM output with the results from the 8 models in spite of these biases (Figs. 3 and 2).

3.4 Comparison of ToE(O_2) with ToE(T)

Are changes in O_2 detectable earlier than warming in the thermocline? We examine this question with the help of Fig. 6, which shows ToE(T) minus ToE(O_2) for the individual models. In general, temperature changes are detectable before O_2 changes in around 64 ± 11 % of the thermocline (yellow to brown colours in Fig. 6). As discussed in section 3.1, the anthropogenic O_2 signal emerges late or not at all in many low latitude regions, while the anthropogenic warming signal is emerging in most regions and typically early around the equator. However, there are also areas where anthropogenic deoxygenation is detectable earlier than anthropogenic warming in all models (green to blue colours in Fig. 6). These cover 35 ± 11 % of the global thermocline in the nine models. They are mainly located in the mid latitudes, especially between $\sim 15°$ N and 30° N in the North Pacific, around Antarctica (including the Ross and Weddell Sea), along the Western Australian Current and the Pacific southern subtropical gyre region. Model results for the Atlantic are mixed. Some models suggest O_2 changes to be detectable earlier than T changes in the subtropical gyres (HadGEM2 and the IPSL family), whereas in other models the O_2 signal does not even emerge.

A mechanistic explanation of early or late emergence of the O_2 signal relative to the temperature signal is not straightforward as two ratios (S/N) are involved. Nevertheless, changes in apparent oxygen utilisation (Δ[-AOU]; Fig. 7) provide some insight into underlying mechanisms. We use Δ[-AOU] as a proxy for changes in water mass age and ventilation as noted in Sect 2.2.

https://doi.org/10.5194/bg-2019-339
Preprint. Discussion started: 3 September 2019


Biogeosciences Discussions Open Access EGU

It is striking that regions with early emergence of anthropogenic O_2 compared to T show typically a decrease in [-AOU] in the future (Fig. 6 versus Fig. 7). [-AOU] is decreasing in 77±8 % of the areas with early emergence of O_2, while only 22±8 % of these regions show an increase in [-AOU] (Fig. 8; blue). On the other hand, [-AOU] is increasing in most of the regions (62±12 %) where T is emerging before O_2 (Fig. 8; green). We interpret these results as follows. A decrease in [-AOU] suggests that the ventilation of the thermocline is decreasing. Under global warming, this can be due to an increase in surface stratification (not shown; see also Gnanadesikan et al., 2007). In turn, the supply rate of O_2 from the surface is decreasing, and consequently thermocline [O_2] and [-AOU] are both decreasing inducing a strong and thus early detectable anthropogenic deoxygenation. At the same time, a decrease in ventilation tends to slow down the penetration of the anthropogenic warming signal from the surface into the thermocline, and similarly the penetration of the thermally driven O_2 signal ([$O_{2,\,sol}$]). The detection of these signals is thus delayed compared to AOU and this may partly counteract the effect of ventilation on the early detection of O_2. There are some exceptions to this mechanism. For example, the GFDL models simulate an increase in [-AOU] around 30° S - 120° W, while O_2 emerges before T. The GFDL models simulate weak warming and even some cooling in this part of the thermocline (Fig. S4), moderate T variability (Fig. S3) and, therefore, no or late emergence of the warming signal (Fig. 2). Thus, in this special case, the early emergence of O_2 relative to T is due to the absence of large warming in a region with noticeable temperature variability.

Regions where the warming signal is detectable before the deoxygenation are typically associated with an increase in [-AOU]. Such increase counteracts the decrease in [$O_{2,\,sol}$], leading to small changes in [O_2], which are thus often not detectable. There are again a few exceptions. For example, the IPSL models simulate a decrease in [-AOU] in the northern North Pacific, but an earlier ToE for T than for O_2 in this region.

In summary, temperature is in general detectable earlier than anthropogenic O_2. However, there are large ocean regions where anthropogenic O_2 changes are detectable earlier in the thermocline in all models. Early emergence of deoxygenation relative to warming is typically detected in regions where thermocline ventilation and [-AOU] are decreasing over the simulation and late emergence of O_2 changes where ventilation and [-AOU] are increasing.

https://doi.org/10.5194/bg-2019-339
Preprint. Discussion started: 3 September 2019

4 Discussion and conclusions

We analysed the time of emergence (ToE) of human-induced changes in oxygen (O_2) concentrations and temperature (T) in the thermocline (200 – 600 m) using nine Earth system model simulations of the climate over the historical and the future period. Using ToE as a metric allows for the assessment of anthropogenic changes by comparing the magnitude of the anthropogenic trend with the magnitude of natural variability. Both these magnitudes vary among models, e.g., due to different climate sensitivities, and this metric was thus found to be relatively strongly model-dependent. Here, we introduced a new metric, the relative ToE (ToE_{rel}), to better compare ToE across different models and variables. ToE_{rel} is computed by subtracting the global mean ToE from the ToE field. Absolute years of emergence are thus not considered by this metric and it only illustrates whether a signal emerges relatively early or late within a model. We investigated whether anthropogenic T or O_2 changes emerge first and link patterns in ToE(T)-ToE(O_2) to changes in apparent oxygen utilisation (Δ[-AOU]) and ventilation of the thermocline. In addition, we also identified the processes for earlier/later detection in O_2 changes compared to temperature changes.

A short-coming of our study is that all the Earth system models included have a relatively coarse resolution for simulating the complex processes in the O_2 minimum zones (Margolskee et al., 2019). Perhaps not surprising, Earth System models diverge in projecting physical and biogeochemical changes in these regions (Brandt et al. 2015; Cabré et al. 2015). Some models used in this study project a large increase in [-AOU] (Fig. 7) and considerable warming (Fig. S6) in the eastern tropical Atlantic, likely indicative of an increasing ventilation (Gnanadesikan et al., 2007). Observations show a decrease in O_2 and an expansion of hypoxia in the tropics (Stramma et al., 2008, 2012) over recent decades, contradicting the long-term projections from some models. However, these observed trends in the tropics may also be a result of natural variability acting on multi-decadal timescales associated with the Pacific Decadal Oscillation.

Comparing ToE estimates from different studies is delicate due to the model and method dependencies of ToE. Hameau et al. (2019) showed that ideally the noise (N) component of ToE should be estimated from simulations that include natural variability forced by explosive volcanic eruptions and changes in total solar irradiance, especially when assessing regional to global scale ToE estimates. However, these authors also find that on a grid cell scale, internal natural variability is typically the dominant contribution to overall natural variability during the last millennium. Therefore, estimating the noise from control simulations that include internal natural variability only, as done in this study, appears justified.

Another limitation of our study lies in the assumption that the anthropogenic signal emerges from interannual to multidecadal variability. The anthropogenic signal S and the noise N is estimated by smoothing the model output with a multi-decadal spline filter. Any potential natural centennial variations are retained in the signal S and removed from the noise N. Results from a forced simulation over the past millennium with CESM1.0 show that potential biases in ToE arising from the neglect of long-term natural variability are small for this model (Hameau et al., 2019). However, our multi-model analysis reveals centennial variations in some grid cells and models causing multiple emergence of the signal from the noise (Fig. A1). This may bias the

https://doi.org/10.5194/bg-2019-339
Preprint. Discussion started: 3 September 2019

detection of the anthropogenic signal towards early emergence. Here, we constrained detection to partly circumvent problems with re-emerging signals; we require that the trend of the signal at the time of emergence must have the same sign as the change between the last and first 30 model years. Re-emerging signals are found in only a few grid cells, except in HadGEM2, and centennial natural variability appears to play a minor role in these simulations. We expect therefore that our estimates of ToE are reliable for the model ensemble.

Published studies addressing the detection of anthropogenic ocean warming focus on the sea surface temperature. To our knowledge, only a single study Hameau et al. (2019) using output from a single model is assessing ToE(T) in the thermocline. Yet, the thermocline is habitat for many fish and other species. Warming in combination with other stressors such as deoxygenation, ocean acidification and hypocapnia, may reduce marine life habitat suitability and extent (e.g. Deutsch et al., 2015; Gattuso et al., 2015; Breitburg et al., 2018; Cheung et al., 2018).

We find that thermocline anthropogenic warming emerges first in low latitudes, followed by the Southern Ocean and the high northern latitudes. No emergence is detected in parts of the subtropical gyres of the Pacific and Indian Ocean. The rapid emergence at low latitudes is explained by the small internal natural variability, but moderate warming signals. Exceptions are the subtropical gyres in the Atlantic and the eastern equatorial Pacific, where it takes approximately two additional decades to detect the temperature changes, mainly because of the relatively large internal natural variability there. The warming in mid- to high latitude thermocline emerges approximately 60 to 80 years later than in low latitudes. No emergence is simulated for the Pacific and Indian subtropical gyres, because the changes in temperature are relatively small and the internal natural variability relatively high there (in accordance with Hameau et al., 2019). For comparison, surface temperature changes emerge at first in low latitudes and then in midlatitudes (Henson et al., 2017).

The time of emergence pattern of thermocline oxygen changes is almost opposite to the one of temperature. Rapid emergence for O_2 is simulated at midlatitudes, whereas low latitudes generally do not experience emergence of the O_2 signal by the end of the 21st century (Rodgers et al., 2015; Frölicher et al., 2016; Long et al., 2016). Even though the internal natural variability is low in the tropical regions, the O_2 signal does not emerge from the noise, because the changes projected by the models are even smaller. This is due to the opposite responses of O_2 components. The thermal component is simulated to decrease (due to temperature increase), but [-AOU] is on average projected to increase, counteracting the $O_{2,\,sol}$ trend (Frölicher et al., 2009; Cocco et al., 2013; Bopp et al., 2017). Some regions show similar relative ToE but for different reasons. For example, in the North Pacific subtropical gyre and the Southern Ocean, both the oxygen depletion and the natural variability are strong. In the Arabian Sea, natural variability and anthropogenic response are both rather weak. Nevertheless, the S/N ratio results in very similar relative ToE for all these regions.

Comparing ToE across models is not straightforward. For example, the transient climate response of the individual models and therefore the ocean heat uptake, thermocline warming and deoxygenation can be highly different (Bopp et al., 2013). In

https://doi.org/10.5194/bg-2019-339
Preprint. Discussion started: 3 September 2019

addition, the simulated internal natural variability largely differs across models (e.g. Resplandy et al., 2015; Frölicher et al., 2016). The CESM1.0, for example, shows very different absolute ToE values for oxygen and temperature compared to other models, mostly due to a very weak internal natural variability (Hameau et al., 2019). We partly resolved these inter-model discrepancies by introducing a new metric, the relative time of emergence. By normalising the ToE using the global averaged ToE as reference allows for a more direct comparison with the other models. As a result, the patterns and time of emergence of anthropogenic changes in O_2 and warming in CESM1.0 are more coherent with the other models for ToE_{rel} than for the raw (absolute) ToE.

Following Hameau et al. (2019), we compared the ToE(T) with the ToE(O_2). We find that in most of the thermocline, the anthropogenic increase in temperature is expected to emerge before anthropogenic O_2 changes. However, in 35$\pm$11 % of the global ocean the O_2 signal emerges before the temperature signal. In the Pacific subtropical gyres, the Southern Ocean and the West Australian Current, the O_2 signal emerges before the temperature signal in all 9 models. Thus, our multi-model analysis confirms earlier findings using output from a single model only (Hameau et al., 2019). The early emergence of O_2 suggests that the monitoring of biogeochemical variables would be particularly useful to detect early signals of anthropogenic change (Joos et al., 2003). Multi-tracer observations of both physical and biogeochemical variables may enable an earlier detection of potential changes than temperature-only data (Keller et al., 2015) in specific regions and for specific processes.

Hameau et al. (2019) established a direct link between the early emergence in O_2 with a slow down of ventilation. A weaker ventilation leads to a decrease in [-AOU], and therefore to a reduction in O_2, with a minor role for organic matter export changes in their simulation. We used [-AOU] as a ventilation age proxy for our model ensemble and concluded that the slow down of the ventilation induces O_2 changes to be detectable before T changes in many regions. A slower ventilation seems to shift the balance between O_2 supply from the surface and O_2 consumption by organic matter remineralisation. Moreover, a more stratified upper ocean delays the propagation of the temperature signal from the surface into the subsurface waters. Note that the exact locations of early O_2 emergence and reductions in [-AOU] and ventilation diverge between the models. This is partly due to model biases in terms of ocean dynamics. In addition, the use of depth coordinates to define a thermocline layer from 200 – 600 m may lead in our analysis to the inclusion of different water masses for different models. Another approach would be to perform the analysis on isopycnal levels instead on depth levels.

To conclude, normalising ToE across models (relative ToE) or estimating ToE in relation to another variable (ToE(T) - ToE(O_2)), reduces the multi-model spread arising from method and model dependencies. We find that in about 35% of the thermocline anthropogenic O_2 depletion emerges before anthropogenic warming. This relative early emergence of O_2 is linked to a more sluggish ventilation of these subsurface waters under global warming. Our study also suggests that temperatures in the thermocline have already left the bounds of natural variability in much of the tropical ocean and that temperatures will have left these bounds in most of the thermocline by 2100 under unabated global warming.

https://doi.org/10.5194/bg-2019-339
Preprint. Discussion started: 3 September 2019

Biogeosciences Discussions Open Access EGU

Data availability. The CMIP5 simulations are available on https://esgf-node.ipsl.upmc.fr. The CESM1.0 simulations are available upon request.

5 Figures

https://doi.org/10.5194/bg-2019-339
Preprint. Discussion started: 3 September 2019

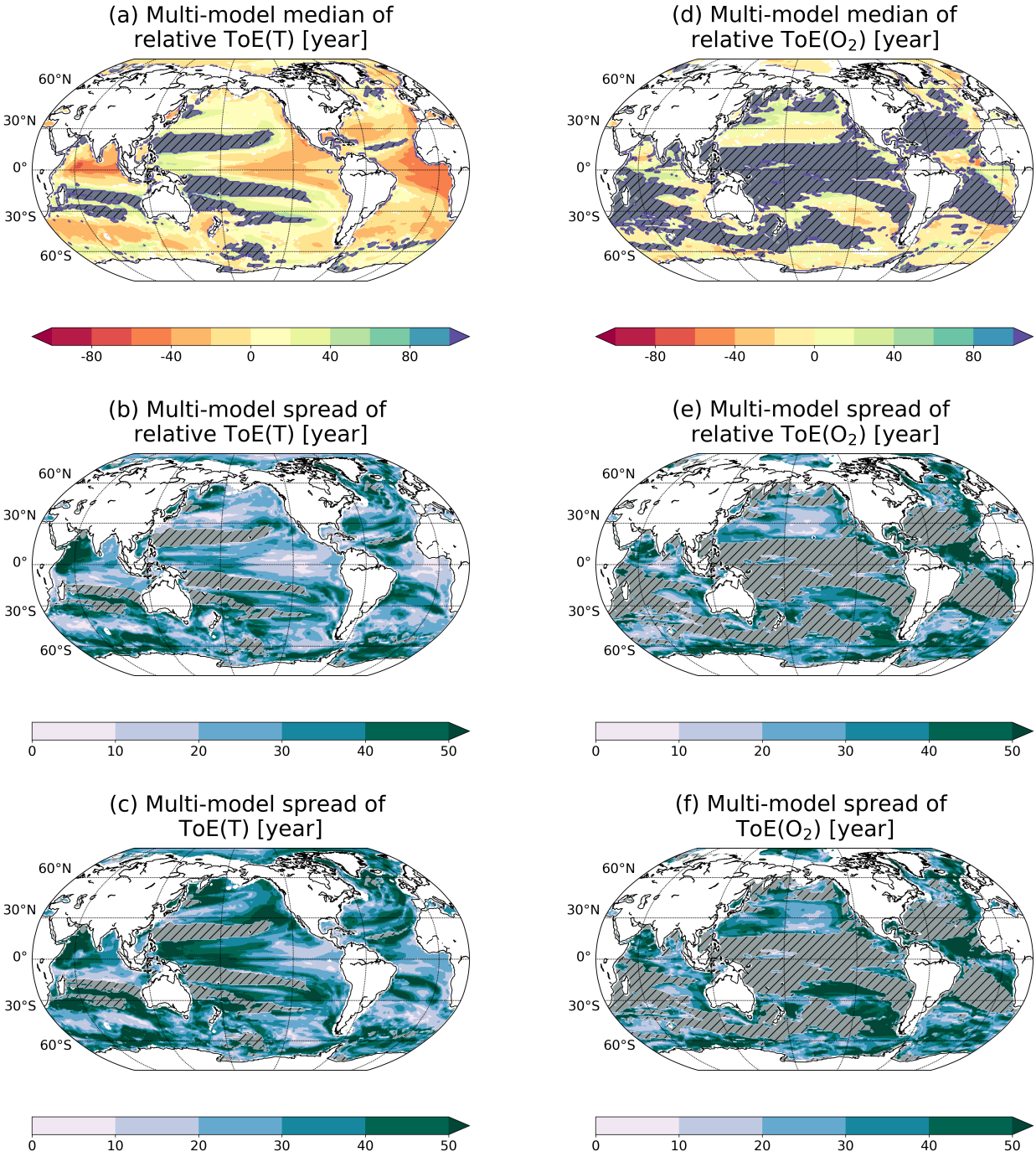

Figure 1. Multi-model median (top panel) and spread (middle panel) of relative ToE for temperature (left column) and dissolved oxygen (right column) for the thermocline (200 – 600 m). The spread is computed as the interquartile range. Multi-model spread of (lower panel) absolute ToE estimates for (c) temperature and (f) dissolved oxygen. The hatched areas show regions with no emergence for at least 3 models. For temperature (oxygen), the relative ToE estimates are shown for each model in Fig. 2 (3) and the absolute estimates in Fig. S1 (S2).

https://doi.org/10.5194/bg-2019-339
Preprint. Discussion started: 3 September 2019

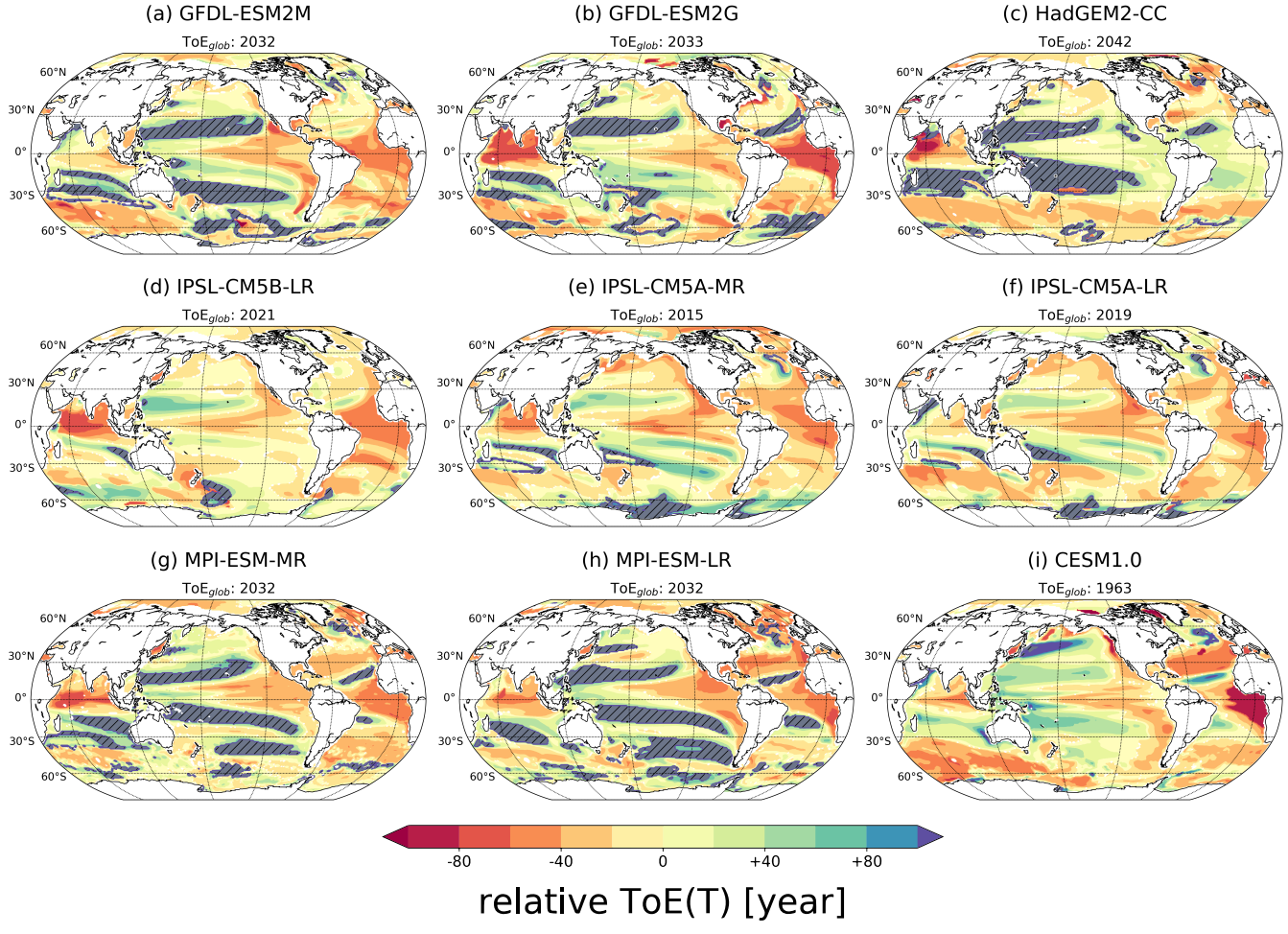

Figure 2. Time of Emergence (ToE) of T in the thermocline (200 – 600 m) relative to the averaged ToE in that layer for each simulation. The hatched areas show regions with no emergence by the end of the 21st century.The values of the global average ToE, ToE$_{glob}$, are given above each panel. The absolute ToE estimates are shown in Fig. S1.

https://doi.org/10.5194/bg-2019-339
Preprint. Discussion started: 3 September 2019

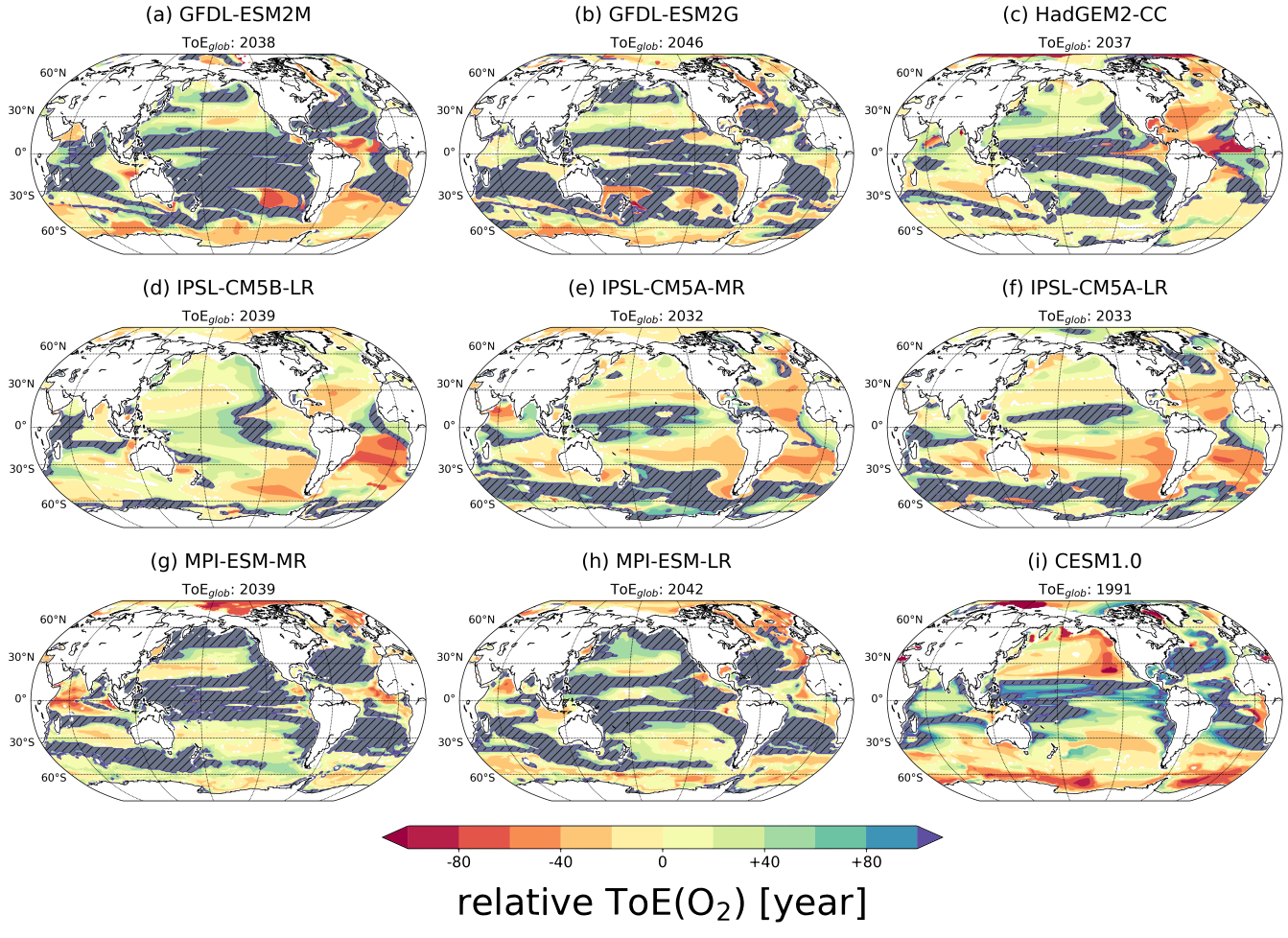

Figure 3. Time of Emergence (ToE) of O_2 in the thermocline (200 – 600 m) relative to the averaged ToE in that layer for each simulation. The hatched areas show regions with no emergence by the end of the 21st century. The absolute ToE estimates are shown in Fig. S2. The global average ToE, ToE$_{glob}$, is shown for each model

https://doi.org/10.5194/bg-2019-339
Preprint. Discussion started: 3 September 2019

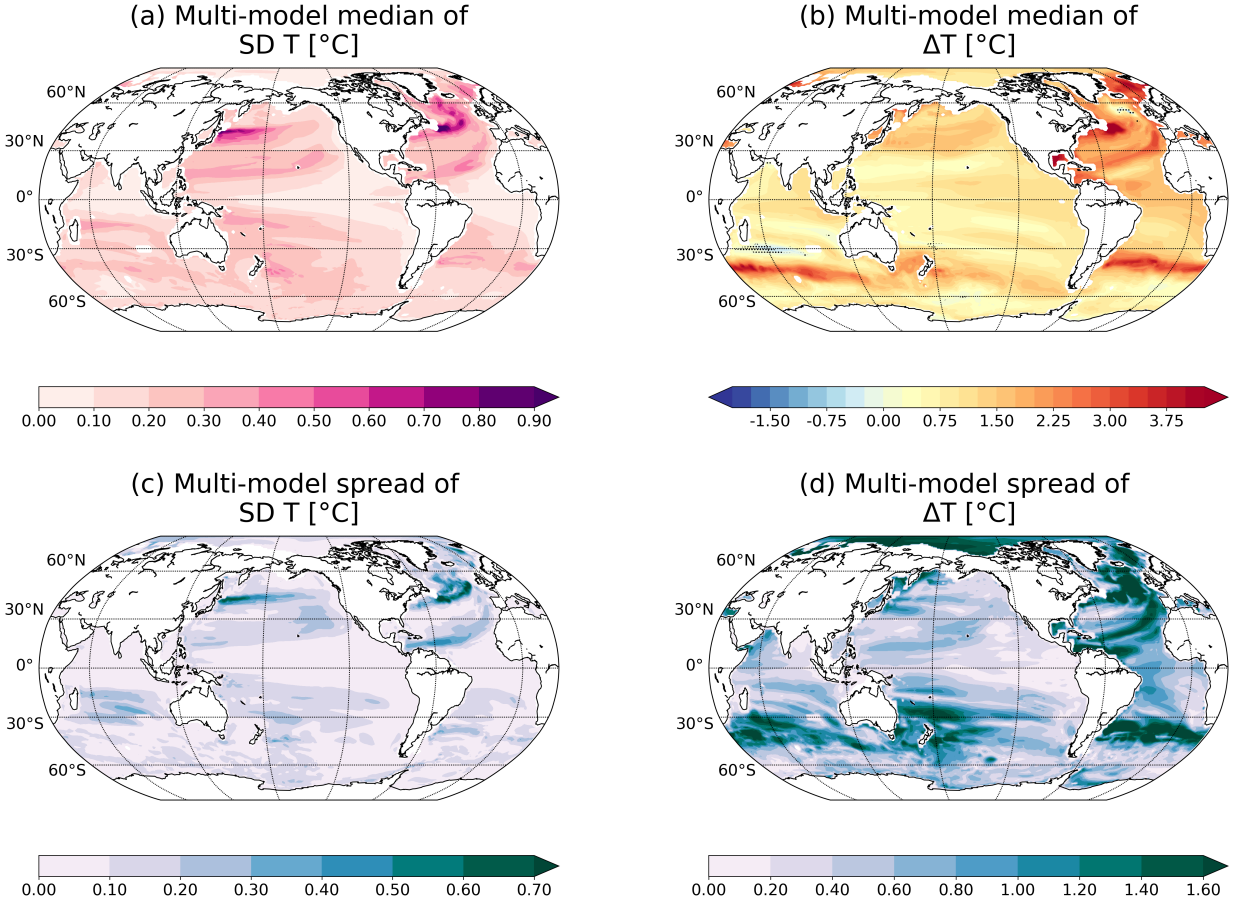

Figure 4. Median (top panels) and spread (bottom panels) of multi-model natural variability (standard deviation of control simulation; left panels) and changes by the end of the 21st century (right panels) of ocean temperature between 200 and 600 m. The individual responses for each model are shown in Figs. S3 and S4.

https://doi.org/10.5194/bg-2019-339
Preprint. Discussion started: 3 September 2019

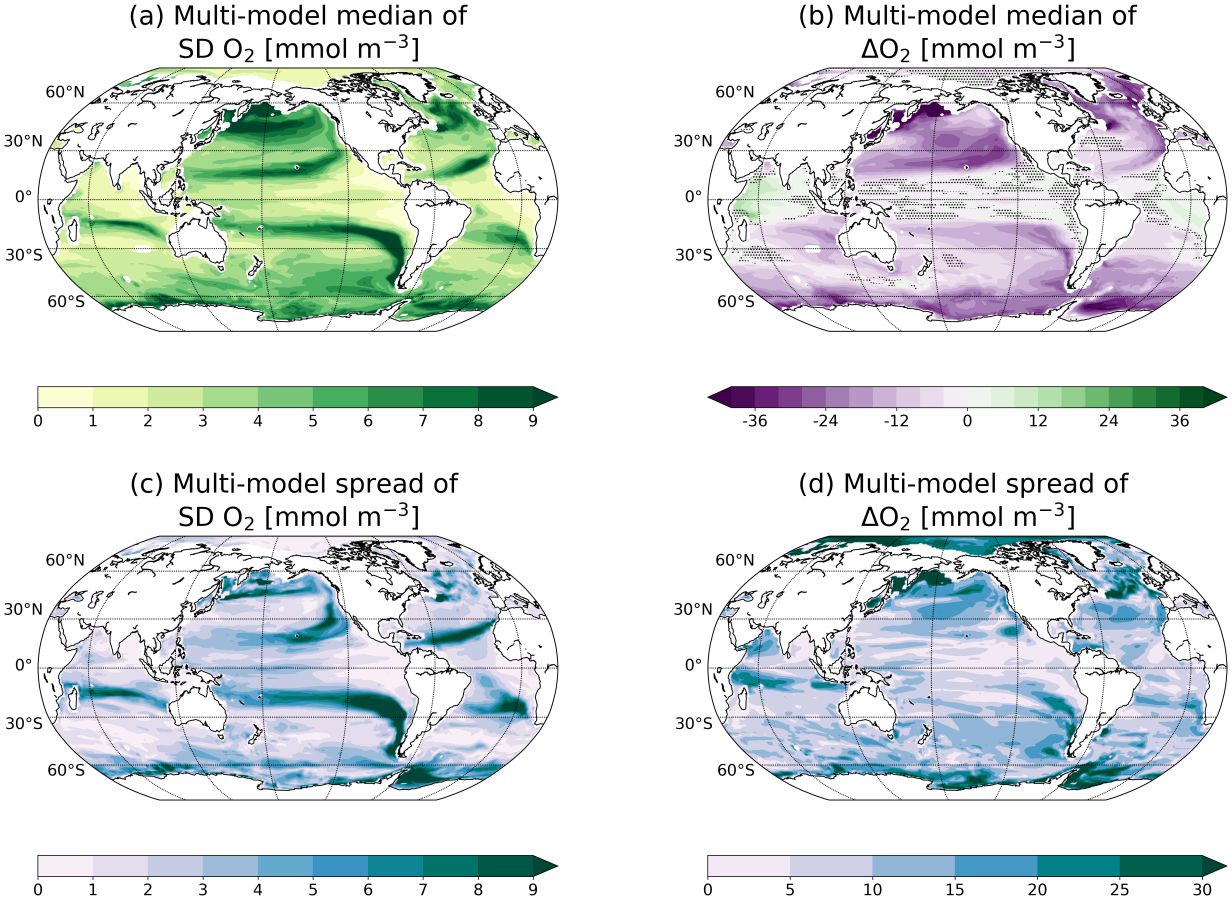

Figure 5. Median (top panels) and spread (bottom panels) of multi-model natural variability (standard deviation of control simulations; left panels) and changes by the end of the 21st century (right panels) of O_2 between 200 and 600 m. The hatched areas in panel b show regions where at least 70% of the models do not agree on ΔO_2 sign. The individual responses for each model are shown in Figs. S5 and S6.

https://doi.org/10.5194/bg-2019-339
Preprint. Discussion started: 3 September 2019

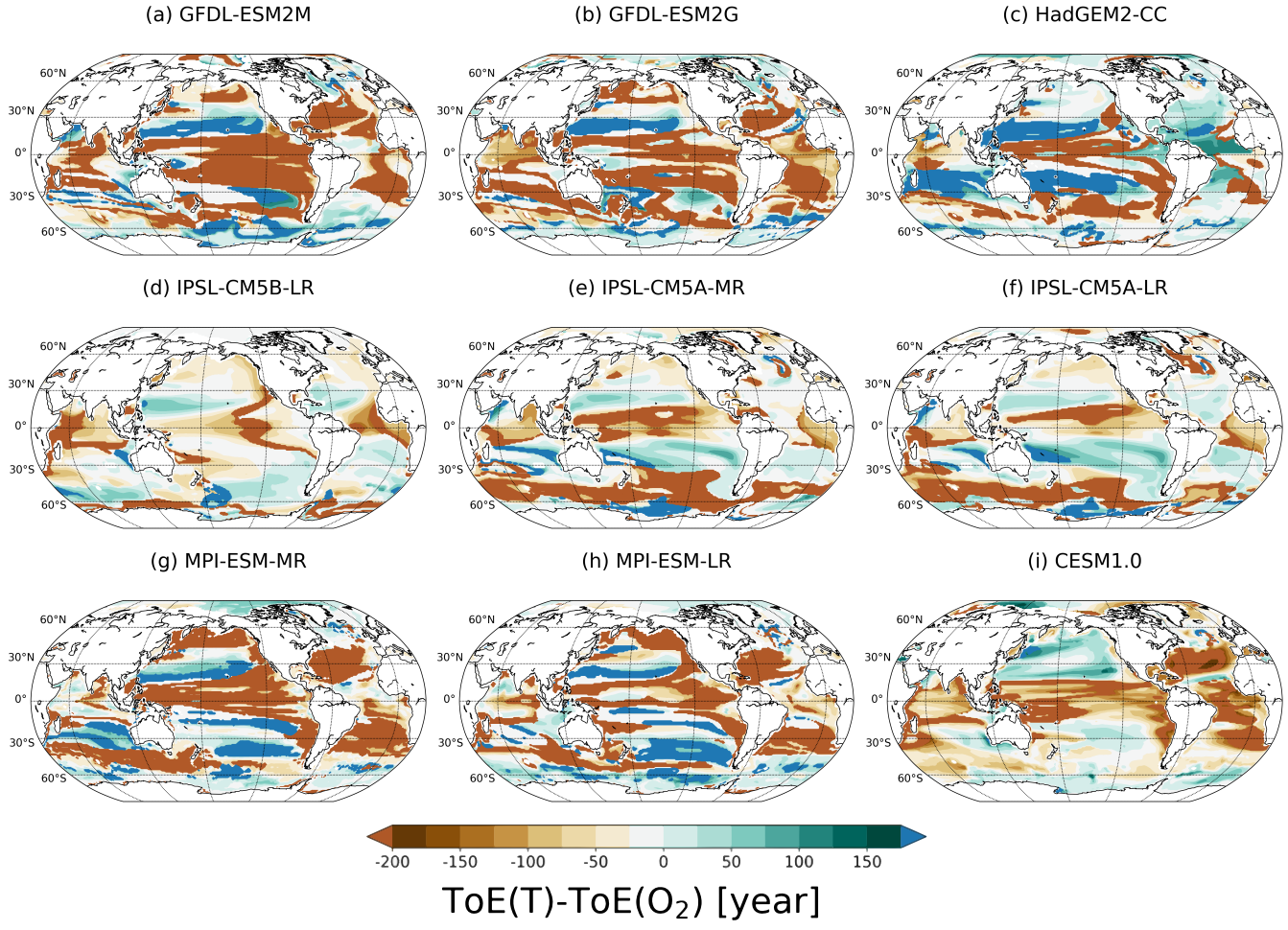

Figure 6. ToE(T) minus ToE(O_2) for each simulation in the thermocline. Blueish colours indicate earlier emergence of oxygen. Brownish colours indicate earlier emergence of temperature. The saturated colours mean that one of the variables has not emerged by 2099.

https://doi.org/10.5194/bg-2019-339
Preprint. Discussion started: 3 September 2019

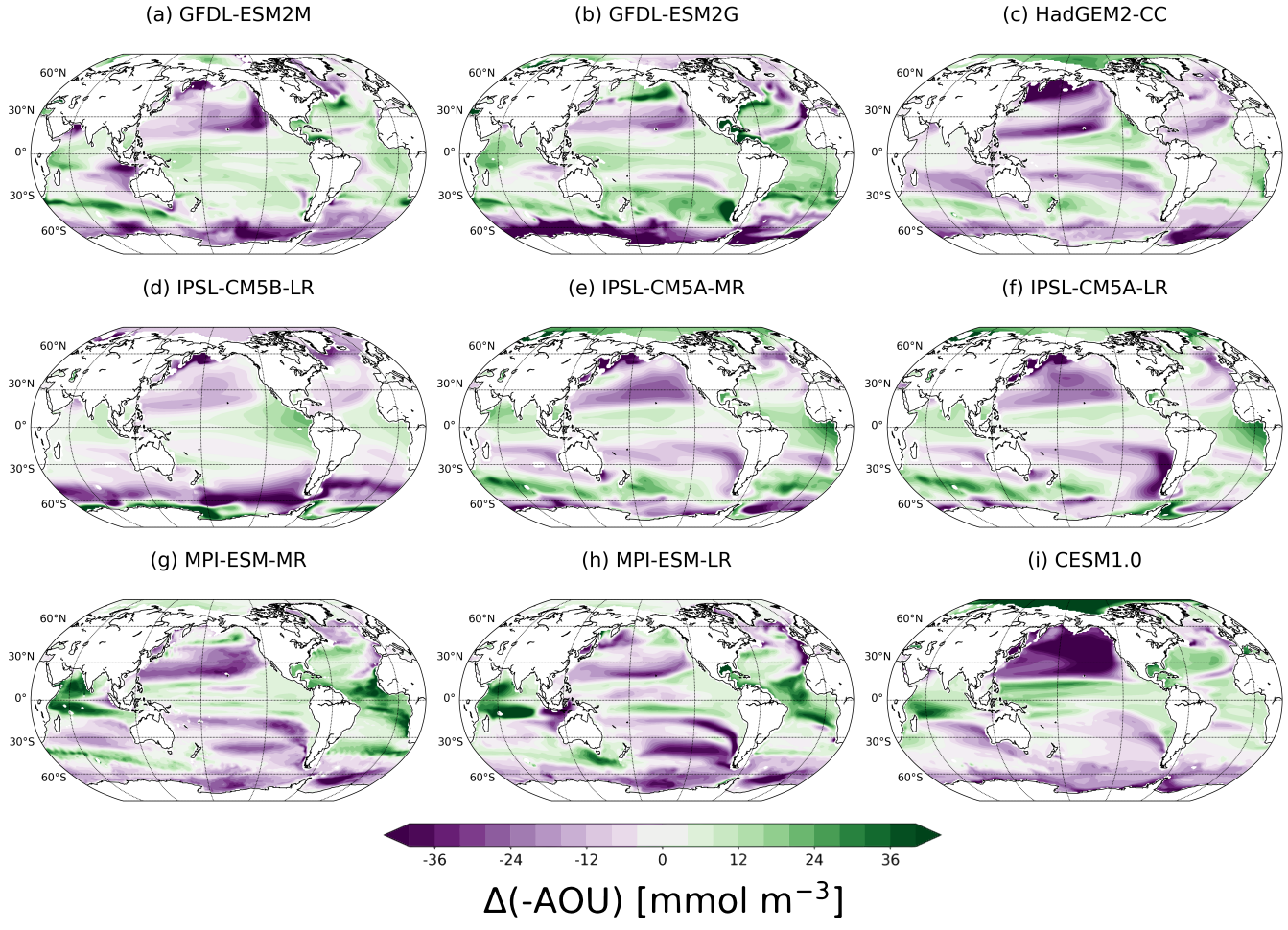

Figure 7. Anthropogenic changes ((2070-2099 CE) minus (1861-1959 CE)) in [-AOU] in the thermocline for each model.

https://doi.org/10.5194/bg-2019-339
Preprint. Discussion started: 3 September 2019

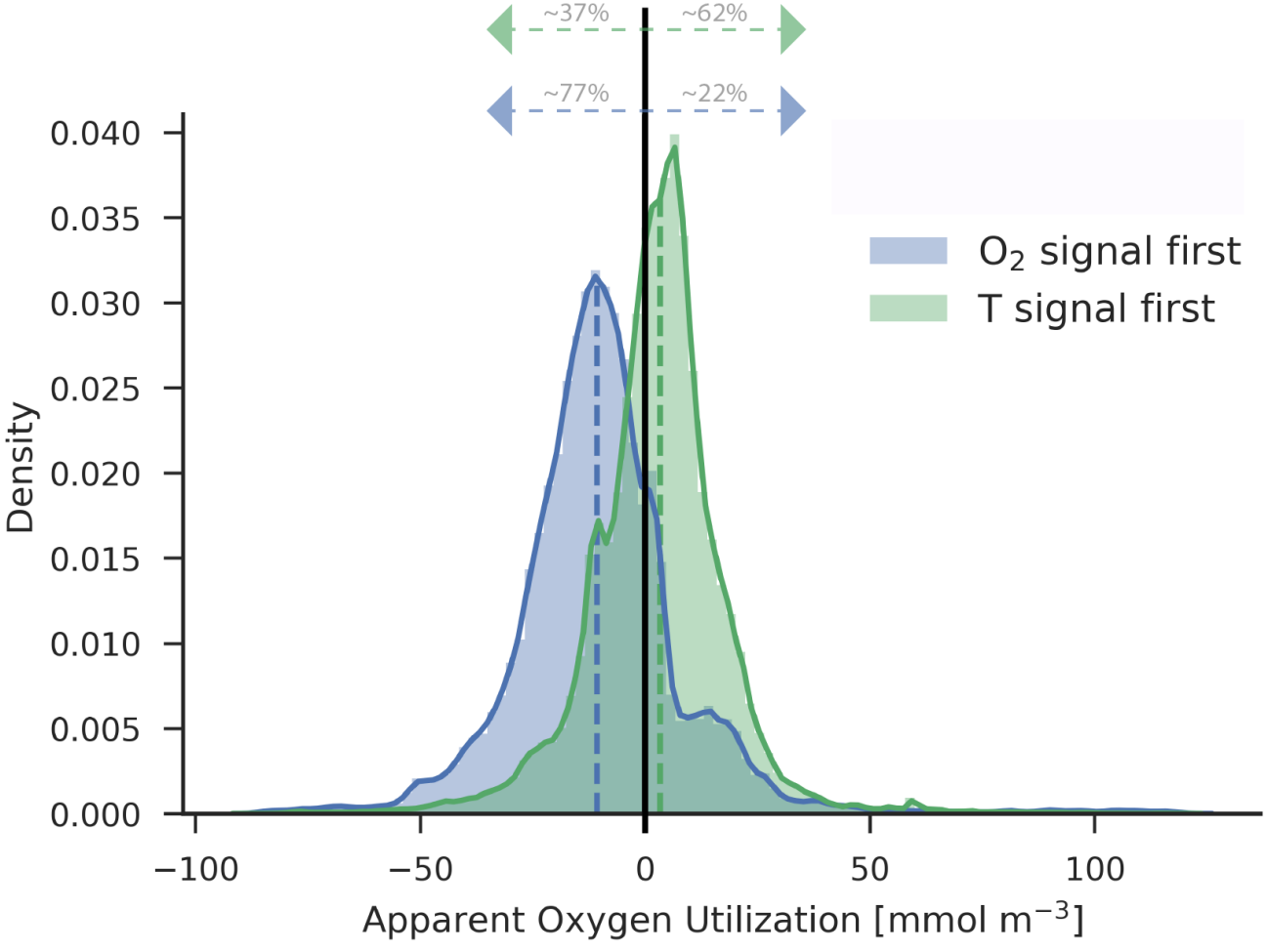

Figure 8. Density distribution of [-AOU] changes by 2099 for the grid points where the O_2 signal emerges first (blue) and where the temperature signal emerges first (green) in the thermocline for the ensemble of 9 models. Each distribution is centred around the median (dashed blue: -10.8 $\mathrm{mmol\ m^{-3}}$; dashed green: 3.3 $\mathrm{mmol\ m^{-3}}$).

https://doi.org/10.5194/bg-2019-339
Preprint. Discussion started: 3 September 2019

Biogeosciences
Discussions
Open Access
EGU

Table 1. Overview of the Earth system models used in this study, their configurations and vertical and approximated horizontal resolutions.

Earth system model	Physical ocean model	Biogeochemical ocean model	Vertical and horizontal ocean resolution
CESM1.0	POP2 (Smith et al., 2010;	BEC (Moore et al., 2002, 2004)	60 levels
Hurrell et al. (2013)	Danabasoglu et al., 2011)		~1° x 1°
GFDL-ESM2M	MOM4p1 (Griffies et al., 2011)	TOPAZ2 (Dunne et al., 2013)	50 levels
GFDL-ESM2G	GOLD (Hallberg, 1997)		~1° x 1°
Dunne et al. (2012, 2013)			
HadGEM2-CC	HadGEM2 (Collins et al., 2011)	HadOCC (Palmer and Totterdell, 2001)	40 levels
Collins et al. (2011)			~2° x 2°
IPSL-CM5A-LR			31 levels
IPSL-CM5A-MR	OPA (Madec et al., 2017)	PISCES (Aumont and Bopp, 2006)	~2° x 2°
IPSL-CM5B-LR			
Dufresne et al. (2013)			
MPI-ESM-LR			40 levels
	MPIOM (Jungclaus et al., 2013)	HAMOCC5.2 (Ilyina et al., 2013)	~1.5° x 1.5°
MPI-ESM-MR			40 levels
			~0.4° x 0.4°
Giorgetta et al. (2013)			

https://doi.org/10.5194/bg-2019-339
Preprint. Discussion started: 3 September 2019

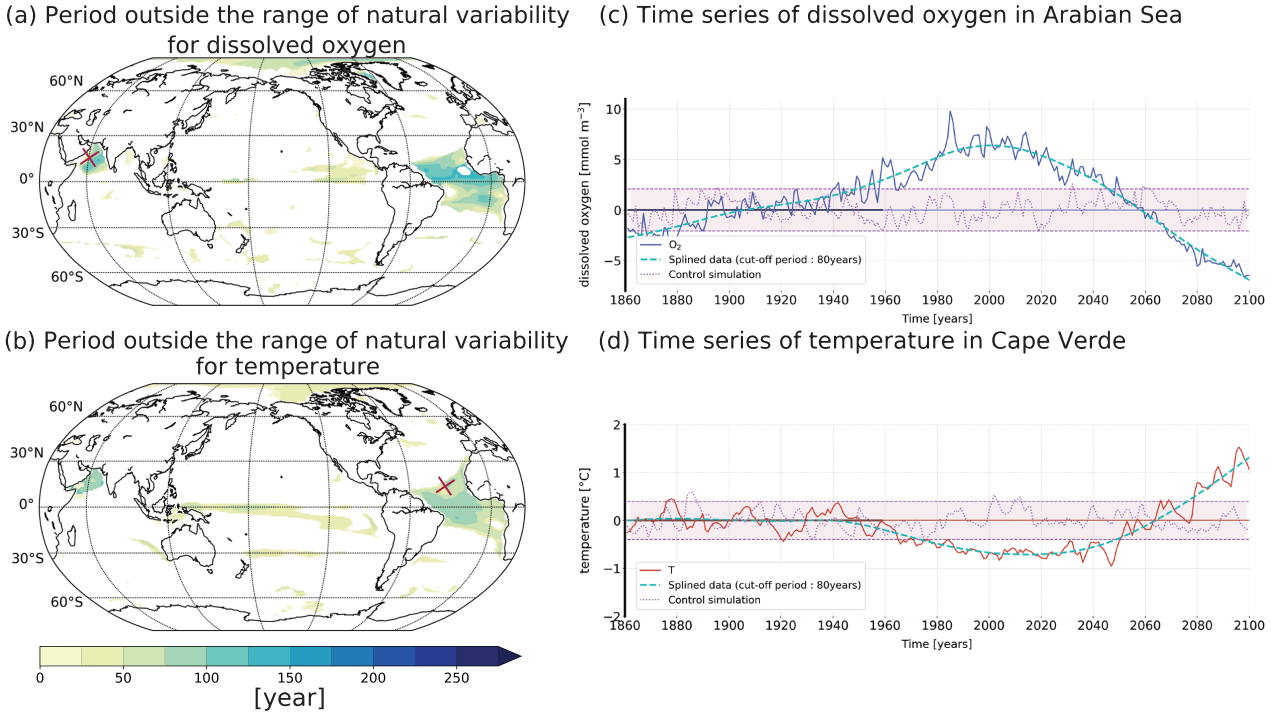

Figure A1. Period outside the range of natural variability for (a) oxygen concentration and (b) temperature in the thermocline for the model HadGEM2. The time series show two example of the temporal evolution of the oxygen concentration (c) and temperature (d) for a single grid point (red crosses in the left panels: Arabian Sea (c) and equatorial Atlantic (d)).

https://doi.org/10.5194/bg-2019-339
Preprint. Discussion started: 3 September 2019

Author contributions. All authors contributed to the discussion and the writing of the paper.

Competing interests. The authors declare that they have no conflict of interest.

Acknowledgements. A. Hameau, F. Joos and T. Frölicher thank the Oeschger Center for Climate Change Research, the Swiss National Science Foundation (#200020_172476 and PP00P2_ 170687) and the H2020 project COMFORT for financial support and the CSCS Swiss National Supercomputing Center for computing resources. We thank C. Raible and F. Lehner for providing CESM output. We also thank the World Climate Research Programme's Working Group on coupled Modelling, which is responsible for CMIP5, and the climate modelling groups for producing and making available their model output.

https://doi.org/10.5194/bg-2019-339
Preprint. Discussion started: 3 September 2019

References

Aumont, O. and Bopp, L.: Globalizing results from ocean in situ iron fertilization studies, Global Biogeochemical Cycles, 20, https://doi.org/10.1029/2005GB002591, https://agupubs.onlinelibrary.wiley.com/doi/abs/10.1029/2005GB002591, 2006.

Battaglia, G. and Joos, F.: Hazards of decreasing marine oxygen: the near-term and millennial-scale benefits of meeting the Paris climate targets, Earth System Dynamics, 9, 797, 2018.

Bilbao, R. A. F., Gregory, J. M., Bouttes, N., Palmer, M. D., and Stott, P.: Attribution of ocean temperature change to anthropogenic and natural forcings using the temporal, vertical and geographical structure, Climate Dynamics, https://doi.org/10.1007/s00382-019-04910-1, https://doi.org/10.1007/s00382-019-04910-1, 2019.

Bopp, L., Le Quéré, C., Heimann, M., Manning, A. C., and Monfray, P.: Climate-induced oceanic oxygen fluxes: Implications for the contemporary carbon budget, Global Biogeochemical Cycles, 16, 6–1, https://doi.org/10.1029/2001GB001445, http://onlinelibrary.wiley.com/doi/10.1029/2001GB001445/abstract, 2002.

Bopp, L., Resplandy, L., Orr, J. C., Doney, S. C., Dunne, J. P., Gehlen, M., Halloran, P., Heinze, C., Ilyina, T., Séférian, R., Tjiputra, J., and Vichi, M.: Multiple stressors of ocean ecosystems in the 21st century: projections with CMIP5 models, Biogeosciences, 10, 6225–6245, https://doi.org/10.5194/bg-10-6225-2013, http://www.biogeosciences.net/10/6225/2013/, 2013.

Bopp, L., Resplandy, L., Untersee, A., Mezo, P. L., and Kageyama, M.: Ocean (de)oxygenation from the Last Glacial Maximum to the twenty-first century: insights from Earth System models, Phil. Trans. R. Soc. A, 375, 20160 323, https://doi.org/10.1098/rsta.2016.0323, http://rsta.royalsocietypublishing.org/content/375/2102/20160323, 2017.

Brandt, P., Bange, H. W., Banyte, D., Dengler, M., Didwischus, S.-H., Fischer, T., Greatbatch, R. J., Hahn, J., Kanzow, T., Karstensen, J., Körtzinger, A., Krahmann, G., Schmidtko, S., Stramma, L., Tanhua, T., and Visbeck, M.: On the role of circulation and mixing in the ventilation of oxygen minimum zones with a focus on the eastern tropical North Atlantic, Biogeosciences, 12, 489–512, https://doi.org/10.5194/bg-12-489-2015, http://www.biogeosciences.net/12/489/2015/, tO READ, 2015.

Breitburg, D., Levin, L. A., Oschlies, A., Grégoire, M., Chavez, F. P., Conley, D. J., Garçon, V., Gilbert, D., Gutiérrez, D., Isensee, K., Jacinto, G. S., Limburg, K. E., Montes, I., Naqvi, S. W. A., Pitcher, G. C., Rabalais, N. N., Roman, M. R., Rose, K. A., Seibel, B. A., Telszewski, M., Yasuhara, M., and Zhang, J.: Declining oxygen in the global ocean and coastal waters, Science, 359, eaam7240, https://doi.org/10.1126/science.aam7240, http://science.sciencemag.org/content/359/6371/eaam7240, 2018.

Cabré, A., Marinov, I., Bernardello, R., and Bianchi, D.: Oxygen minimum zones in the tropical Pacific across CMIP5 models: mean state differences and climate change trends, Biogeosciences, 12, 5429–5454, https://doi.org/10.5194/bg-12-5429-2015, http://www.biogeosciences.net/12/5429/2015/, 2015.

Chen, X. and Tung, K.-K.: Global surface warming enhanced by weak Atlantic overturning circulation, Nature, 559, 387–391, https://doi.org/10.1038/s41586-018-0320-y, https://www.nature.com/articles/s41586-018-0320-y, 2018.

Cheng, L., Trenberth, K. E., Fasullo, J., Boyer, T., Abraham, J., and Zhu, J.: Improved estimates of ocean heat content from 1960 to 2015, Science Advances, 3, e1601 545, https://doi.org/10.1126/sciadv.1601545, https://advances.sciencemag.org/content/3/3/e1601545, 2017.

Cheng, L., Abraham, J., Hausfather, Z., and Trenberth, K. E.: How fast are the oceans warming?, Science, 363, 128–129, https://doi.org/10.1126/science.aav7619, https://science.sciencemag.org/content/363/6423/128, 2019.

Cheung, W. W., Jones, M. C., Reygondeau, G., and Frölicher, T. L.: Opportunities for climate-risk reduction through effective fisheries management, Global change biology, 24, 5149–5163, 2018.

https://doi.org/10.5194/bg-2019-339
Preprint. Discussion started: 3 September 2019

Cheung, W. W. L., Dunne, J., Sarmiento, J. L., and Pauly, D.: Integrating ecophysiology and plankton dynamics into projected maximum fisheries catch potential under climate change in the Northeast Atlantic, ICES Journal of Marine Science, 68, 1008–1018, https://doi.org/10.1093/icesjms/fsr012, https://academic.oup.com/icesjms/article/68/6/1008/699298, 2011.

Christensen, J., Hewitson, B., A. Busuioc, A. Chen, X. Gao, I. Held, R. Jones, R.K. Kolli, W.-T. Kwon, R. Laprise, V. Magaña Rueda, L. Mearns, C.G. Menéndez, J. Räisänen, A. Rinke, A. Sarr, and P. Whetton: Regional Climate Projections. In: Climate Change 2007: The Physical Science Basis. Contribution of Working Group I to the Fourth Assessment Report of the Intergovernmental Panel on Climate Change, Cambridge University Press, Cambridge, United Kingdom and New York, NY, USA., 2007.

Cocco, V., Joos, F., Steinacher, M., Froelicher, T. L., Bopp, L., Dunne, J., Gehlen, M., Heinze, C., Orr, J., Oschlies, A., Schneider, B., Segschneider, J., and Tjiputra, J.: Oxygen and indicators of stress for marine life in multi-model global warming projections, Biogeosciences, 10, 1849–1868, https://doi.org/10.5194/bg-10-1849-2013, wOS:000317010600040, 2013.

Collins, W. J., Bellouin, N., Doutriaux-Boucher, M., Gedney, N., Halloran, P., Hinton, T., Hughes, J., Jones, C. D., Joshi, M., Liddicoat, S., Martin, G., O'Connor, F., Rae, J., Senior, C., Sitch, S., Totterdell, I., Wiltshire, A., and Woodward, S.: Development and evaluation of an Earth-System model – HadGEM2, Geoscientific Model Development, 4, 1051–1075, https://doi.org/https://doi.org/10.5194/gmd-4-1051-2011, https://www.geosci-model-dev.net/4/1051/2011/, 2011.

Danabasoglu, G., Bates, S. C., Briegleb, B. P., Jayne, S. R., Jochum, M., Large, W. G., Peacock, S., and Yeager, S. G.: The CCSM4 Ocean Component, Journal of Climate, 25, 1361–1389, https://doi.org/10.1175/JCLI-D-11-00091.1, https://journals.ametsoc.org/doi/abs/10.1175/JCLI-D-11-00091.1, 2011.

Deutsch, C., Ferrel, A., Seibel, B., Pörtner, H.-O., and Huey, R. B.: Climate change tightens a metabolic constraint on marine habitats, Science, 348, 1132–1135, https://doi.org/10.1126/science.aaa1605, http://science.sciencemag.org/content/348/6239/1132, 2015.

Dufresne, J.-L., Foujols, M.-A., Denvil, S., Caubel, A., Marti, O., Aumont, O., Balkanski, Y., Bekki, S., Bellenger, H., Benshila, R., Bony, S., Bopp, L., Braconnot, P., Brockmann, P., Cadule, P., Cheruy, F., Codron, F., Cozic, A., Cugnet, D., de Noblet, N., Duvel, J.-P., Ethé, C., Fairhead, L., Fichefet, T., Flavoni, S., Friedlingstein, P., Grandpeix, J.-Y., Guez, L., Guilyardi, E., Hauglustaine, D., Hourdin, F., Idelkadi, A., Ghattas, J., Joussaume, S., Kageyama, M., Krinner, G., Labetoulle, S., Lahellec, A., Lefebvre, M.-P., Lefevre, F., Levy, C., Li, Z. X., Lloyd, J., Lott, F., Madec, G., Mancip, M., Marchand, M., Masson, S., Meurdesoif, Y., Mignot, J., Musat, I., Parouty, S., Polcher, J., Rio, C., Schulz, M., Swingedouw, D., Szopa, S., Talandier, C., Terray, P., Viovy, N., and Vuichard, N.: Climate change projections using the IPSL-CM5 Earth System Model: from CMIP3 to CMIP5, Climate Dynamics, 40, 2123–2165, https://doi.org/10.1007/s00382-012-1636-1, https://doi.org/10.1007/s00382-012-1636-1, 2013.

Dunne, J. P., John, J. G., Adcroft, A. J., Griffies, S. M., Hallberg, R. W., Shevliakova, E., Stouffer, R. J., Cooke, W., Dunne, K. A., Harrison, M. J., Krasting, J. P., Malyshev, S. L., Milly, P. C. D., Phillipps, P. J., Sentman, L. T., Samuels, B. L., Spelman, M. J., Winton, M., Wittenberg, A. T., and Zadeh, N.: GFDL's ESM2 Global Coupled Climate–Carbon Earth System Models. Part I: Physical Formulation and Baseline Simulation Characteristics, Journal of Climate, 25, 6646–6665, https://doi.org/10.1175/JCLI-D-11-00560.1, https://journals.ametsoc.org/doi/full/10.1175/JCLI-D-11-00560.1, 2012.

Dunne, J. P., John, J. G., Shevliakova, E., Stouffer, R. J., Krasting, J. P., Malyshev, S. L., Milly, P. C. D., Sentman, L. T., Adcroft, A. J., Cooke, W., Dunne, K. A., Griffies, S. M., Hallberg, R. W., Harrison, M. J., Levy, H., Wittenberg, A. T., Phillips, P. J., and Zadeh, N.: GFDL's ESM2 Global Coupled Climate–Carbon Earth System Models. Part II: Carbon System Formulation and Baseline Simulation Characteristics, Journal of Climate, 26, 2247–2267, https://doi.org/10.1175/JCLI-D-12-00150.1, https://journals.ametsoc.org/doi/full/10.1175/JCLI-D-12-00150.1, 2013.

https://doi.org/10.5194/bg-2019-339
Preprint. Discussion started: 3 September 2019

Enting, I. G.: On the use of smoothing splines to filter CO2 data, Journal of Geophysical Research: Atmospheres, 92, 10 977–10 984, https://doi.org/10.1029/JD092iD09p10977, http://onlinelibrary.wiley.com/doi/10.1029/JD092iD09p10977/abstract, 1987.

Frame, D., Joshi, M., Hawkins, E., Harrington, L. J., and de Roiste, M.: Population-based emergence of unfamiliar climates, Nature Climate Change, 7, 407–411, https://doi.org/10.1038/nclimate3297, https://www.nature.com/articles/nclimate3297, 2017.

Frölicher, T. L. and Paynter, D. J.: Extending the relationship between global warming and cumulative carbon emissions to multi-millennial timescales, Environmental Research Letters, 10, 075 002, https://doi.org/10.1088/1748-9326/10/7/075002, http://stacks.iop.org/1748-9326/10/i=7/a=075002, 2015.

Frölicher, T. L., Joos, F., Plattner, G.-K., Steinacher, M., and Doney, S. C.: Natural variability and anthropogenic trends in oceanic oxygen in a coupled carbon cycle–climate model ensemble, Global Biogeochemical Cycles, 23, GB1003, https://doi.org/10.1029/2008GB003316, 2009.

Frölicher, T. L., Rodgers, K. B., Stock, C. A., and Cheung, W. W. L.: Sources of uncertainties in 21st century projections of potential ocean ecosystem stressors, Global Biogeochemical Cycles, 30, 1224–1243, https://doi.org/10.1002/2015GB005338, http://onlinelibrary.wiley.com/doi/10.1002/2015GB005338/full, 2016.

Garcia, H. E. and Gordon, L. I.: Oxygen solubility in seawater: Better fitting equations, Limnology and Oceanography, 37, 1307–1312, https://doi.org/10.4319/lo.1992.37.6.1307, http://onlinelibrary.wiley.com/doi/10.4319/lo.1992.37.6.1307/abstract, 1992.

Gattuso, J.-P., Magnan, A., Billé, R., Cheung, W. W. L., Howes, E. L., Joos, F., Allemand, D., Bopp, L., Cooley, S. R., Eakin, C. M., Hoegh-Guldberg, O., Kelly, R. P., Pörtner, H.-O., Rogers, A. D., Baxter, J. M., Laffoley, D., Osborn, D., Rankovic, A., Rochette, J., Sumaila, U. R., Treyer, S., and Turley, C.: Contrasting futures for ocean and society from different anthropogenic CO2 emissions scenarios, Science, 349, aac4722, https://doi.org/10.1126/science.aac4722, http://science.sciencemag.org/content/349/6243/aac4722, 2015.

Giorgetta, M. A., Jungclaus, J., Reick, C. H., Legutke, S., Bader, J., Böttinger, M., Brovkin, V., Crueger, T., Esch, M., Fieg, K., Glushak, K., Gayler, V., Haak, H., Hollweg, H.-D., Ilyina, T., Kinne, S., Kornblueh, L., Matei, D., Mauritsen, T., Mikolajewicz, U., Mueller, W., Notz, D., Pithan, F., Raddatz, T., Rast, S., Redler, R., Roeckner, E., Schmidt, H., Schnur, R., Segschneider, J., Six, K. D., Stockhause, M., Timmreck, C., Wegner, J., Widmann, H., Wieners, K.-H., Claussen, M., Marotzke, J., and Stevens, B.: Climate and carbon cycle changes from 1850 to 2100 in MPI-ESM simulations for the Coupled Model Intercomparison Project phase 5, Journal of Advances in Modeling Earth Systems, 5, 572–597, https://doi.org/10.1002/jame.20038, https://agupubs.onlinelibrary.wiley.com/doi/full/10.1002/jame.20038, 2013.

Gnanadesikan, A., Russell, J. L., and Zeng, F.: How does ocean ventilation change under global warming?, Ocean Science, 3, 43–53, https://hal.archives-ouvertes.fr/hal-00298310, 2007.

Gnanadesikan, A., Dunne, J. P., and John, J.: Understanding why the volume of suboxic waters does not increase over centuries of global warming in an Earth System Model, Biogeosciences, 9, 1159–1172, https://doi.org/https://doi.org/10.5194/bg-9-1159-2012, https://www.biogeosciences.net/9/1159/2012/, 2012.

Griffies, S. M., Winton, M., Donner, L. J., Horowitz, L. W., Downes, S. M., Farneti, R., Gnanadesikan, A., Hurlin, W. J., Lee, H.-C., Liang, Z., Palter, J. B., Samuels, B. L., Wittenberg, A. T., Wyman, B. L., Yin, J., and Zadeh, N.: The GFDL CM3 Coupled Climate Model: Characteristics of the Ocean and Sea Ice Simulations, Journal of Climate, 24, 3520–3544, https://doi.org/10.1175/2011JCLI3964.1, https://journals.ametsoc.org/doi/full/10.1175/2011JCLI3964.1, 2011.

Hallberg, R.: Some aspects of the circulation in ocean basins with isopycnals intersecting sloping boundaries., 1997.

Hameau, A., Mignot, J., and Joos, F.: Assessment of time of emergence of anthropogenic deoxygenation and warming: insights from a CESM simulation from 850 to 2100 CE, Biogeosciences, 16, 1755–1780, https://doi.org/https://doi.org/10.5194/bg-16-1755-2019, 2019.

https://doi.org/10.5194/bg-2019-339
Preprint. Discussion started: 3 September 2019

Han, W., Vialard, J., McPhaden, M. J., Lee, T., Masumoto, Y., Feng, M., and de Ruijter, W. P.: Indian Ocean Decadal Variability: A Review, Bulletin of the American Meteorological Society, 95, 1679–1703, https://doi.org/10.1175/BAMS-D-13-00028.1, https://journals.ametsoc.org/doi/full/10.1175/BAMS-D-13-00028.1, 2014.

Hauri, C., Gruber, N., McDonnell, A. M. P., and Vogt, M.: The intensity, duration, and severity of low aragonite saturation state events on the California continental shelf, Geophysical Research Letters, 40, 3424–3428, https://doi.org/10.1002/grl.50618, https://agupubs.onlinelibrary.wiley.com/doi/abs/10.1002/grl.50618, 2013.

Hawkins, E. and Sutton, R.: Time of emergence of climate signals, Geophysical Research Letters, 39, L01 702, https://doi.org/10.1029/2011GL050087, http://onlinelibrary.wiley.com/doi/10.1029/2011GL050087/abstract, 2012.

Henson, S. A., Beaulieu, C., and Lampitt, R.: Observing climate change trends in ocean biogeochemistry: when and where, Global Change Biology, 22, 1561–1571, https://doi.org/10.1111/gcb.13152, http://onlinelibrary.wiley.com/doi/10.1111/gcb.13152/abstract, 2016.

Henson, S. A., Beaulieu, C., Ilyina, T., John, J. G., Long, M., Séférian, R., Tjiputra, J., and Sarmiento, J. L.: Rapid emergence of climate change in environmental drivers of marine ecosystems, Nature Communications, 8, 14 682, https://doi.org/10.1038/ncomms14682, http://www.nature.com/ncomms/2017/170307/ncomms14682/full/ncomms14682.html, 2017.

Hurrell, J. W., Holland, M. M., Gent, P. R., Ghan, S., Kay, J. E., Kushner, P. J., Lamarque, J.-F., Large, W. G., Lawrence, D., Lindsay, K., Lipscomb, W. H., Long, M. C., Mahowald, N., Marsh, D. R., Neale, R. B., Rasch, P., Vavrus, S., Vertenstein, M., Bader, D., Collins, W. D., Hack, J. J., Kiehl, J., and Marshall, S.: The Community Earth System Model: A Framework for Collaborative Research, Bulletin of the American Meteorological Society, 94, 1339–1360, https://doi.org/10.1175/BAMS-D-12-00121.1, http://journals.ametsoc.org/doi/abs/10.1175/BAMS-D-12-00121.1, 2013.

Ilyina, T., Six, K. D., Segschneider, J., Maier-Reimer, E., Li, H., and Núñez-Riboni, I.: Global ocean biogeochemistry model HAMOCC: Model architecture and performance as component of the MPI-Earth system model in different CMIP5 experimental realizations, Journal of Advances in Modeling Earth Systems, 5, 287–315, https://doi.org/10.1029/2012MS000178, https://agupubs.onlinelibrary.wiley.com/doi/abs/10.1029/2012MS000178, 2013.

Joos, F., Plattner, G.-K., Stocker, T. F., Körtzinger, A., and Wallace, D. W. R.: Trends in marine dissolved oxygen: Implications for ocean circulation changes and the carbon budget, Eos, Transactions American Geophysical Union, 84, 197–201, https://doi.org/10.1029/2003EO210001, http://onlinelibrary.wiley.com/doi/10.1029/2003EO210001/abstract, 2003.

Jungclaus, J. H., Fischer, N., Haak, H., Lohmann, K., Marotzke, J., Matei, D., Mikolajewicz, U., Notz, D., and von Storch, J. S.: Characteristics of the ocean simulations in the Max Planck Institute Ocean Model (MPIOM) the ocean component of the MPI-Earth system model, Journal of Advances in Modeling Earth Systems, 5, 422–446, https://doi.org/10.1002/jame.20023, https://agupubs.onlinelibrary.wiley.com/doi/full/10.1002/jame.20023, 2013.

Keller, K. M., Joos, F., and Raible, C. C.: Time of emergence of trends in ocean biogeochemistry, Biogeosciences, 11, 3647–3659, https://doi.org/10.5194/bg-11-3647-2014, 2014.

Keller, K. M., Joos, F., Lehner, F., and Raible, C. C.: Detecting changes in marine responses to ENSO from 850 to 2100 C.E.: Insights from the ocean carbon cycle, Geophysical Research Letters, 42, 2014GL062 398, https://doi.org/10.1002/2014GL062398, http://onlinelibrary.wiley.com/doi/10.1002/2014GL062398/abstract, 2015.

Lehner, F., Joos, F., Raible, C. C., Mignot, J., Born, A., Keller, K. M., and Frölicher, T. L.: Climate and carbon cycle dynamics in a CESM simulation from 850 to 2100 CE, Earth System Dynamics, 6, 411–434, https://doi.org/10.5194/esd-6-411-2015, http://www.earth-syst-dynam.net/6/411/2015/, 2015.

https://doi.org/10.5194/bg-2019-339
Preprint. Discussion started: 3 September 2019

Levitus, S., Antonov, J. I., Boyer, T. P., Locarnini, R. A., Garcia, H. E., and Mishonov, A. V.: Global ocean heat content 1955-2008 in light of recently revealed instrumentation problems, Geophysical Research Letters, 36, L07 608, https://doi.org/10.1029/2008gl037155, <GotoISI>://000265101500001, 2009.

Levitus, S., Antonov, J. I., Boyer, T. P., Baranova, O. K., Garcia, H. E., Locarnini, R. A., Mishonov, A. V., Reagan, J. R., Seidov, D., Yarosh, E. S., and Zweng, M. M.: World ocean heat content and thermosteric sea level change (0–2000 m), 1955–2010, Geophysical Research Letters, 39, https://doi.org/10.1029/2012GL051106, https://agupubs.onlinelibrary.wiley.com/doi/abs/10.1029/2012GL051106, 2012.

Lombardozzi, D., Bonan, G. B., and Nychka, D. W.: The emerging anthropogenic signal in land–atmosphere carbon-cycle coupling, Nature Climate Change, 4, 796–800, https://doi.org/10.1038/nclimate2323, https://www.nature.com/articles/nclimate2323, 2014.

Long, M. C., Deutsch, C., and Ito, T.: Finding forced trends in oceanic oxygen, Global Biogeochemical Cycles, 30, 2015GB005 310, https://doi.org/10.1002/2015GB005310, http://onlinelibrary.wiley.com/doi/10.1002/2015GB005310/abstract, 2016.

Madec, G., Bourdallé-Badie, R., Bouttier, P.-A., Bricaud, C., Bruciaferri, D., Calvert, D., Chanut, J., Clementi, E., Coward, A., Delrosso, D., Ethé, C., Flavoni, S., Graham, T., Harle, J., Iovino, D., Lea, D., Lévy, C., Lovato, T., Martin, N., Masson, S., Mocavero, S., Paul, J., Rousset, C., Storkey, D., Storto, A., and Vancoppenolle, M.: NEMO ocean engine, https://doi.org/10.5281/zenodo.3248739, https://zenodo.org/record/3248739#.XRX3H-gzZPY, 2017.

Magnan, A. K., Colombier, M., Billé, R., Joos, F., Hoegh-Guldberg, O., Pörtner, H.-O., Waisman, H., Spencer, T., and Gattuso, J.-P.: Implications of the Paris agreement for the ocean, Nature Climate Change, 6, 732–735, https://doi.org/10.1038/nclimate3038, https://www.nature.com/articles/nclimate3038, 2016.

Margolskee, A., Frenzel, H., Emerson, S., and Deutsch, C.: Ventilation Pathways for the North Pacific Oxygen Deficient Zone, Global Biogeochemical Cycles, 33, 875–890, https://doi.org/10.1029/2018GB006149, https://agupubs.onlinelibrary.wiley.com/doi/full/10.1029/2018GB006149, 2019.

Matear, R. J. and Hirst, A. C.: Long-term changes in dissolved oxygen concentrations in the ocean caused by protracted global warming, Global Biogeochemical Cycles, 17, n/a–n/a, https://doi.org/10.1029/2002GB001997, http://doi.wiley.com/10.1029/2002GB001997, 2003.

Moore, J. K., Doney, S. C., Kleypas, J. A., Glover, D. M., and Fung, I. Y.: An intermediate complexity marine ecosystem model for the global domain, Deep-Sea Research Part II: Topical Studies in Oceanography, 49, 403–462, https://doi.org/10.1016/S0967-0645(01)00108-4, 2002.

Moore, J. K., Doney, S. C., and Lindsay, K.: Upper ocean ecosystem dynamics and iron cycling in a global three-dimensional model, Global Biogeochemical Cycles, 18, GB4028, https://doi.org/10.1029/2004GB002220, http://onlinelibrary.wiley.com/doi/10.1029/2004GB002220/abstract, 2004.

Palmer, J. R. and Totterdell, I. J.: Production and export in a global ocean ecosystem model, Deep Sea Research Part I: Oceanographic Research Papers, 48, 1169–1198, https://doi.org/10.1016/S0967-0637(00)00080-7, http://www.sciencedirect.com/science/article/pii/S0967063700000807, 2001.

Pörtner, H.-O., Karl, D. M., Boyd, P. W., Cheung, W., Lluch-Cota, S. E., Nojiri, Y., Schmidt, D. N., Zavialov, P. O., Alheit, J., and Aristegui, J.: Ocean systems, in: Climate change 2014: impacts, adaptation, and vulnerability. Part A: global and sectoral aspects. contribution of working group II to the fifth assessment report of the intergovernmental panel on climate change, pp. 411–484, Cambridge University Press, 2014.

Resplandy, L., Séférian, R., and Bopp, L.: Natural variability of CO2 and O2 fluxes: What can we learn from centuries-long climate models simulations?, Journal of Geophysical Research: Oceans, 120, 384–404, https://doi.org/10.1002/2014JC010463, http://onlinelibrary.wiley.com/doi/10.1002/2014JC010463/abstract, 2015.

Rhein, M., Rintoul, S. R., Aoki, S., Campos, E., Chambers, D., Feely, R. A., Gulev, S., Johnson, G. C., Josey, S. A., Kostianoy, A., Mauritzen, C., Roemmich, D., and Talley, L. D.: Observations: Ocean, in: Climate Change 2013: The Physical Science Basis. Contribution of Working Group I to the Fifth Assessment Report of the Intergovernmental Panel on Climate Change, edited by Stocker, T. F., Qin, D., Plattner, G.-K., Tignor, M., Allen, S. K., Boschung, J., Nauels, A., Xia, Y., Bex, V., and Midgley, P. M., pp. 255–316, Cambridge University Press, https://eprints.soton.ac.uk/362480/, 2013.

Riahi, K., Rao, S., Krey, V., Cho, C., Chirkov, V., Fischer, G., Kindermann, G., Nakicenovic, N., and Rafaj, P.: RCP 8.5—A scenario of comparatively high greenhouse gas emissions, Climatic Change, 109, 33, https://doi.org/10.1007/s10584-011-0149-y, https://doi.org/10.1007/s10584-011-0149-y, 2011.

Rodgers, K. B., Lin, J., and Frölicher, T. L.: Emergence of multiple ocean ecosystem drivers in a large ensemble suite with an Earth system model, Biogeosciences, 12, 3301–3320, https://doi.org/10.5194/bg-12-3301-2015, https://www.biogeosciences.net/12/3301/2015/, 2015.

Roemmich, D., Church, J., Gilson, J., Monselesan, D., Sutton, P., and Wijffels, S.: Unabated planetary warming and its ocean structure since 2006, Nature Climate Change, 5, 240–245, https://doi.org/10.1038/nclimate2513, https://www.nature.com/articles/nclimate2513, 2015.

Sarmiento, J. L., Hughes, T. M. C., Stouffer, R. J., and Manabe, S.: Simulated response of the ocean carbon cycle to anthropogenic climate warming, Nature, 393, 245, https://doi.org/10.1038/30455, https://www.nature.com/articles/30455, 1998.

Schmidtko, S., Stramma, L., and Visbeck, M.: Decline in global oceanic oxygen content during the past five decades, Nature, 542, 335–339, https://doi.org/10.1038/nature21399, http://www.nature.com/nature/journal/v542/n7641/full/nature21399.html, 2017.

Smith, R., Jones, P., Briegleb, B., Bryan, F., Danabasoglu, G., Dennis, J., Dukowicz, J., Eden, C., Fox-Kemper, B., and Gent, P.: The parallel ocean program (POP) reference manual: ocean component of the community climate system model (CCSM) and community earth system model (CESM), Rep. LAUR-01853, 141, 1–140, 2010.

Stramma, L., Johnson, G. C., Sprintall, J., and Mohrholz, V.: Expanding Oxygen-Minimum Zones in the Tropical Oceans, Science, 320, 655–658, https://doi.org/10.1126/science.1153847, http://science.sciencemag.org/content/320/5876/655, 2008.

Stramma, L., Prince, E. D., Schmidtko, S., Luo, J., Hoolihan, J. P., Visbeck, M., Wallace, D. W. R., Brandt, P., and Körtzinger, A.: Expansion of oxygen minimum zones may reduce available habitat for tropical pelagic fishes, Nature Climate Change, 2, 33–37, https://doi.org/10.1038/nclimate1304, http://www.nature.com/nclimate/journal/v2/n1/full/nclimate1304.html, 2012.

Stroeve, J. C., Kattsov, V., Barrett, A., Serreze, M., Pavlova, T., Holland, M., and Meier, W. N.: Trends in Arctic sea ice extent from CMIP5, CMIP3 and observations, Geophysical Research Letters, 39, https://doi.org/10.1029/2012GL052676, https://agupubs.onlinelibrary.wiley.com/doi/abs/10.1029/2012GL052676, 2012.

Taylor, K. E., Stouffer, R. J., and Meehl, G. A.: An Overview of CMIP5 and the Experiment Design, Bulletin of the American Meteorological Society, 93, 485–498, https://doi.org/10.1175/BAMS-D-11-00094.1, https://journals.ametsoc.org/doi/abs/10.1175/BAMS-D-11-00094.1, 2012.

Wang, M. and Overland, J. E.: A sea ice free summer Arctic within 30 years: An update from CMIP5 models, Geophysical Research Letters, 39, https://doi.org/10.1029/2012GL052868, https://agupubs.onlinelibrary.wiley.com/doi/abs/10.1029/2012GL052868, 2012.